Professor Grasemann
Handling Topical Editor, Solid Earth

March 4th 2017

Dear Professor Grasemann

We are grateful for your editorial advice, and the constructive and informative reviews you solicited on our *Solid Earth* discussion paper '*Controls on fault zone structure and brittle fracturing in the foliated hanging-wall of the Alpine Fault'* by Tim Little and Tom Blenkinsop.

All changes and corrections that the reviewers requested, have now been completed and are incorporated into the enclosed manuscript. In this author's response document, we have also copied the reviewers comments and replied to them point-by-point in blue italicised Cambria text.

We thank you for your consideration of the newly revised manuscript and we look forward to hearing from you in the near future.

Yours sincerely

Dr Jack Williams

Dr Jack Williams
Research Associate in Structural Geology
School of Earth and Ocean Sciences
Cardiff University
Main Building
Cardiff
CF10 3AT
Phone: +44 (0)29 2087 4336
Email: JWilliams132@cardiff.ac.uk

Dr Jack Williams
Cysylltiad Ymchwil mewn Daeareg Strwythurol
Ysgol Gwyddorau'r Ddaear a'r Mor
Prifysgol Caerdydd
Prif Adeilad
Caerdydd
CF10 3AT
Ffôn : +44 (0)29 2087 4336
Ebost: JWilliams132@cardiff.ac.uk

Reviewer Number 1

General Comments

Concise and clearly written. The topic is of wide interest, and is introduced well. Some of the figures are too small and/or are poorly labelled. Captions are commonly disorganized, and do not actually describe the content of the different parts of the figure. The photographs, in particular, are commonly not very clear or helpful.

With regards to the reviewer's comments on figures, this partly reflects that their resolution was reduced during the online manuscript upload process. The final manuscript will have much better-quality figures. We have addressed the specific comments that the reviewer has with figures below, and think that these also help with the general concerns raised in this comment.

#1 I would have liked to have seen a physical explanation for why vertical unloading during exhumation should favour the development of the foliation-parallel fractures. The paper does not do this, so citing this scenario as an "explanation" is not particularly convincing.

We acknowledge that there is uncertainty in whether it is unloading and the release of confining pressure during hanging-wall exhumations that forms foliation-parallel fracture per se (e.g. Engleder et al 1985), or if they are generated by other mechanisms such as seismic shaking (as discussed in Townend et al 2017). This is now clarified at lines 358-361.

Nevertheless, the point that these fractures formed at *low confining pressures (regardless of the actual mechanism) is well-founded. Our discussion of the relationship between foliation and rock fracturing takes account of fracture fill and deformation experiments of anisotropic rock (Donath et al 1961, Nasseri et al 2003, Paterson and Wong 2005). These studies find that this relationship depends on (1) the mechanical anisotropy that the foliation imposes (i.e. lithology), (2) the angle between the maximum principal stresses (σ_1) and the foliation, and (3) the confining pressure during rock fracturing (Lines 287-299).*

At Stony Creek, this spatial change of fracturing occurs within the same lithology (Figure 7) leading us to conclude that point 1 cannot be exclusively true (Lines 313-316). The highly variable stress state around the Alpine Fault (e.g. Upton et al 2017) makes it difficult to exclude point (2). However, if the 1-2 km wide network of foliation-parallel fractures extended to appreciable depths, then this should be detected by reductions in seismic velocity (e.g. Jones and Nur 1984). Conversely, the low velocity zone around the Alpine Fault has a width of only 60-200 m (Line 395, Eccles et al 2015). This leaves us to infer that the foliation parallel-fractures have formed in the near-surface at relatively low confining pressures compared to the foliation non-parallel fractures (lines 415-417).

Differences in fracture fill also supports this argument. Foliation-parallel fractures are open with no evidence of offset, so likely formed in tension. In the absence of high pore fluid pressures, this is likely to reflect low confining pressures. Compositional and microstructural analysis of the gouge-fill of fractures not aligned to the foliation indicate that they formed in shear and were subsequently mineralised with phases stable at relatively high temperatures (<400℃, Williams et al. 2017, lines 371). See also comment #1 to reviewer #2

#2 Similarly, the explanation of "development of fault wedges" (where? how?) or dynamic earthquake stressing from below, as causes for variously oriented gouge filled fractures in the damage zone is not well enough discussed or supported, in my opinion.

To keep the manuscript succinct, we did not to go into detail on the mechanisms that can account for variably oriented gouge-filled fractures around the Alpine Fault. Instead we cited previous studies that explain these mechanisms in more detail. However, we have now included more information on these points at lines 378-392.

Specifically, we have described why Alpine Fault thrust wedges may internally deform, which is accommodated by gouge filled fractures. (Cooper and Norris 1994, Norris and Cooper 1995, 1997; lines 378-385), and also the role of dynamic coseismic stresses (Lines 387-392). With regards to the *latter point, Ampuero and Ma (2017) demonstrated that the extent of coseismic damage is influenced by the thickness of the seismogenic crust. Therefore, the relatively thin seismogenic crust around the Alpine Fault (Boese et al. 2012) and its narrow inner damage zone are in good agreement with this point. Again, in the manuscript we also highlight that these are interpretations of our datasets, not full explanations.*

Abstract

Abstract is concise and clearly stated on the whole.

Line 21: Suggest “principal slip zones [of]” is moved ahead of “Alpine Fault”

Corrected (line 20)

Line 38: suggest “rather than the footwall” is added to the end of this sentence.

This sentence was removed during revision of the abstract

Introduction

To the point and well stated.
Goals are clearly identified.

Line 69-70: brackets in brackets

This is unavoidable as we are citing another study in the brackets

Line 74: add “s” to “Alpine fault”’

Corrected (line 75)

Tectonic Setting

Lines 95-100: Along-strike changes in slip rate are not what has led to the tri-partite division of the Alpine fault. This statement is quite misleading.

This statement has been removed (see line 95).

Line 108: replace “form” with “occur in spatial sequence towards the fault” After “(Figure 2)” start a new sentence. At the beginning of this, replace “which are” by “These”.

Corrected (line 102-104)

Line 111: For clarity, insert a comma after “metabasitic mylonites”. Also, the subsequent “or” should be replaced by “and”

Corrected (line 106)

Line 112. Start a new sentence at “reflect” [i.e., “These reflect..”]

Corrected (line 112)

Line 117: Insert “brittle overprint” after “This”

Corrected (Line 111)

Line 122: “projection of outcrops” is unclear in meaning or logic, as written. “Measurements” of what?

We acknowledge that the term "projection of outcrop-derived measurements," is misleading and will be removed. Instead, we are now explicit that the regional orientation of the Alpine Fault reported here is based on the presumption that the foliation should parallel the shear zone boundary in such a high strain zone (lines 119-121). The fault orientation is thus parallel to the average orientation of the mylonitic foliation (e.g. Sibson et al 1981; Norris and Cooper 2007). The fault orientation at depth is also defined from geophysical surveys (Stern et al 2007). We will also note there is some evidence of the Alpine Fault potentially dipping at <62° (Toy et al. 2017).

Why does a seemingly artificial projection process at the surface require a planar zone at >4 km depth? What are the assumptions?

These points were fully addressed by Norris and Cooper (1995) as cited (lines 121-126). Their hypothesis was developed mainly from field mapping, however, it is also supported by sandbox models. In particular, these authors note that the depth extent to which topography can affect the stress field is equal to 1-2x the scale of the valley relief. Given that the valley relief of the Southern Alps immediately adjacent to the Alpine Fault is ~2000 m, then a <4 km joining depth for the partitioned near-surface sections was considered appropriate (Norris and Cooper 1995).

More recent mapping of Alpine Fault surface traces using LiDAR (Barth et al 2012, Langridge et al 2014) and results from numerical modelling (Upton et al 2017) also support the idea that the Alpine Fault is segmented in the near-surface. However, they do indicate that segmentation may only extend as deep as 0.5 km, and we note this too (line 123).

We emphasise that this study does not seek to develop or critically evaluate these models. Rather, these ideas are presented here to justify our methods for estimating the true distance of our field measuring stations from the Alpine Fault (Lines 165). Furthermore, we also account for an end-member case in which the Alpine Fault is not segmented (i.e. it dips at 45° at the surface) and find it does not significantly influence our results (see comment for Line 163).

Line 125: I disagree that the AF necessarily has a dip of 45 degrees at >4 km, or that the data mentioned by the authors demonstrates this, and I note that the statement is not supported by any references.

As noted in the previous comment, we will now explicitly cite the data that support a ~45° dip of the Alpine Fault (Simpson et al 1994, Norris and Cooper 1995, Barth et al 2012, Upton et al 2017), and note the studies that show there is local variation in this (Lines 120-121).

Methodology

In Section 3.1 need to start out by pointing out the known shallow dip of the fault at DFDP-1?

The dip is based on projection of the fault dip at outcrop and that sampled in the boreholes (Townend et al 2013), and this is now noted at line 152.

Line 140: If the DFDP-1 holes are up to 150 m deep, why was only 25 m of core investigated for this study? Explain.

This method requires intervals of both good quality BHTV and CT drill-core images, and which have sufficient fractures (>2 per core section) that could be matched to estimate the rotation required.

Most significantly, only 70 m of drill-core was recovered across the two DFDP-1 boreholes. This entails that significant intervals of the boreholes were not cored (as shown in Figure 3) and so do not have drill-core CT scans. Where core was recovered in DFDP-1A, the BHTV images were of poor quality, so it was not possibly to reliably pick geographically oriented fractures. Conversely, within the relatively intact DFDP-1B footwall (depths >128 m), too few fractures were recognised to allow core reorientation. These points are now address at lines 147-149.

Line 152. Insert comma after “Appendix A”

Corrected, line 153

Line 156. “Distances” is vague. How measured, in what direction?

These are orthogonal distances from the fault trace (line 158)

Line 160: They were measured not “collected”

Corrected, line 159

Line 163: What uncertainties in the measured quantities (e.g., fracture density) are introduced by assuming a generic “thrust” fault dip of exactly 30 when the actual fault dip may be different than that?

It is accepted that there is an inherent uncertainty in our damage zone width estimates given the uncertainty of the orientation of the Alpine Fault at depth (see comment for line 122). We now provide estimates of damage zone width assuming an end-member case in which the fault is not segmented and dips at 45° from the surface (i.e. the regional orientation) in Table S3.

The widest damage zone estimate that this fault dip indicates is 205 m (Havelock Creek) and it is <170 m wide across all other transects. Note, we do not consider the fault dip predicted by DFDP-2B (62°; Toy et al 2017) to be realistic to our field transects. This borehole was sampling the Alpine Fault at distances 1-2 km from the fault, whereas our field transects are all within 500 m of the fault. This result from DFDP-2B may be relevant to the Amethyst Boreholes, as discussed for the reviewers comments for line 180.

Therefore, although the reviewer is correct that there is some uncertainty in our results (which we can account for), this does not unduly influence our interpretation that the Alpine Fault has a relatively narrow inner damage zone. These points are discussed fully at lines 338-344.

Line 164: an extraneous comma.

Corrected, line 166

Line 166: it is a method, not a “methodology”. The “-ology” is a little pretentious, in my opinion.

The word ‘methodology’ was removed during subsequent manuscript revisions (line 171-173).

Line 180: I disagree that Norris and Cooper (1995) demonstrated that the Alpine fault dips c. 45 below the Amythyst tunnel locality. Also, “circa” is a time term, not a spatial or angular term.

As noted for the comment at line 163, we now allow for the full range of possible dips of the Alpine Fault at this locality (30-62°m lines 184-185). These estimates imply that the AHP lies 0.7-2.0 km from the Alpine Fault. We will remove the erroneous use of “circa” and use “~” instead

Line 181: See my statement above regarding line 163 and uncertainties tied to an assumed fault dip.

See reply to above comment

Lines 187-190: “intense fracturing” adjacent to “minor” faults is not measured, nor was it captured in the cores (due to their poor recovery). For the paper, only quite intact cores (i.e., the least fractured intervals) were imaged by CT from which corresponding fracture densities were derived. How representative are these fracture density estimates likely to be? Are they maxima or minima?

Shouldn't this sampling bias be acknowledged and implications for using the results be mentioned?

The main purpose of the AHP CT scans was to investigate fracture orientations ~1 km from the Alpine Fault, not fracture density. As the reviewer notes, any estimates of fracture density we make will be a biased as we only scanned the most intact core. Furthermore, we cannot reliably determine natural from induced fractures in the drill-core (Lines 262-264).

As such, we only describe fracture density in qualitative terms (Figure S4), which consistent with the initial (cited) core descriptions (Geotech et al 2006, Savage 2013). Therefore, we remain confident in the interpretation and analyses we have carried out on fracture orientation.

Lines 198-200: This statement is only true if the top vs. bottom of each piece of core was marked as they came out of the ground. Please elaborate.

The orientations are obtained from drill-core logs and are accurate to ±5° and this is now accounted for (Lines 201). These core logs do not note how the orientation were measured. Nevertheless, the foliation orientations that they report (and the fact this is broadly constant about 060/70 SE), is consistent with orientations obtained from inside the Amethyst Tunnel itself (Savage 2013; Lines 255-257). Furthermore, we are most interested in the angular relationship between fractures and foliation, not the absolute orientations themselves. Our findings are, therefore, not significantly influenced by uncertainty in the true orientation of these fractures.

Line 199: What is the "known orientation," how was it measured, and what are the uncertainties in this assigned dip/ or dip direction?

See reply to previous comment

Results

Line 214: What are the criteria used to distinguish "fractures" from "foliations" in the BHTV? To what degree can one be confident that these criteria "work"? How about your comparison of the BHTV plots with the cores?

In this study, we do not distinguish between fractures and foliation in the BHTV images (except in the cases where fractures in the BHTV images can be directly matched with those recognised in the BHTV images (Figure 4)), and we have revised the text so that it simply refers to BHTV "features' (e.g. lines 221). Indeed, as noted this may explain why there is some difference in the orientations gathered from the CT and BHTV datasets (Line 225).

Line 217: What is meant by "type of fracture"? Vague and unclear. Do you mean "host rock type"?

This is now revised to "fracture fill" (Line 229), which are based on the CT number of the fracture fill and classified in Table 1 of Williams et al. (2016).

Line 221: It would be good and appropriate here to site a statistical measure of fault attitude "clustering" rather simply stating qualitatively that one subset of the data is "more clustered" than the other. The plots are not very convincing on their own.

To quantitatively assess the clustering of fractures around the Alpine Fault, the resultant vector method described in Priest (1993) has now been used. Here, the magnitude of the resultant vector from all fracture orientations is normalised by the number of fractures, with values approaching 1 indicating a high amount of clustering and vice versa. Vectors for individual fractures are weighted by the Terzaghi correction and so there is no misorientation bias in these results.

The results of this analysis are outlined in Table 1 (See also lines 209-215). They indicate that fractures adjacent to the Alpine Fault (i.e. in the DFDP-1 datasets) are less clustered than those ~1-2 km from it (i.e. in the Amethyst Hydro Project, line 258), consistent with qualitative analysis of the stereonets (Figures 5 and 11).

It is not possible to perform such an analysis with the field datasets, as an insufficient number of fracture orientations were measured at each site for a reliable quantification of clustering to be made (Lines 214-215). Furthermore, there are local variations in the foliation orientation between these sites (Figure 7). This means it is not possible to aggregate orientations from multiple sites to quantitatively assess clustering (i.e. since foliation-parallel fractures won't all plot in the same place across different sites). Nevertheless, the trends they qualitatively indicate (that fractures are more clustered further from the fault) are consistent with the DFDP-1 and AHP datasets (line 282). Therefore, we are confident that the field datasets are representative of fractures around the Alpine Fault, and that they can robustly determine the distance from the fault where changes in fracturing style occur.

Line 251: Be exact. This is in the Alpine Schist.

That AHP sampled the Alpine Schist, a sub-member of the Haast Schist, as now stated (Line 253)

Discussion

Lines 269-274.Authors refer to the field-observed fractures at >160 m from fault as being "mostly open." Given they are observed at the face of an outcrop in a high rainfall setting, can one be sure that they do not have gouge in them at depth a short distance below the exposed ground surface? See your lines 258-259. Do youreally know that they are open?

Such weathering of gouge from fractures at the outcrop scale is unlikely to have occurred, as gouge-filled fractures are still frequently observed, even at >160 m from the fault (Figure 8). The point we wish to make is just that fractures of this fill are particularly *abundant <160 m from the fault (See Figure 7). For the reviewers concern to be true, then weathering must have been selective and only affected fractures >160 m from the fault, which seems implausible.*

In the Amethyst road tunnel, which is >160 m from the fault, many of the observed foliation-parallel fractures are gouge filled

The reviewer's observation of foliation parallel gouge-filled fractures in the Amethyst Tunnel is actually consistent with our field observations, which note gouge-filled fractures ~500 m from the fault at Bullock Creek (Figure 8e, line 250). As noted above, it is density of gouge-filled fractures that interests us. Such an observation in the Amethyst Tunnel would only conflict with our results if these fractures were consistently found to have densities of >1 fracture/metre (as noted in lines 261-262, our datasets cannot constrain the ratio of open to filled fractures in AHP drill-core, and we make no attempt to do this).

Lines 306-307: I am unconvinced that the transect data has demonstrated a "confining pressure" cause/effect for foliation-parallel fracturing/or not. This is an interpretation not a fact.

We agree that this should revised to an interpretation, and that other factors may have led to the development of these fractures (Line 358). Also, see reply #1 to this reviewer

Line 332: I have no idea what "broadly oriented" means.

We no longer use the term 'broadly oriented'

Lines 321-322 and Line 331: These statements seem to contradict one another: The fracture density is spatially constant but it isn't(?). Please clarify and be exact and consistent.

The point we wish to make is that total fracture density is relatively constant across our field transects (Lines 320), but that the density of gouge-filled fractures is particularly high within <160 m of the fault (Figure 7, Lines 333). That fractures with a particular fill are used to define damage zone width is not new. See for example Mitchell and Faulkner (2009), who use the density of 'fluid inclusion planes' to define damage zone width and ignored the density of open fractures (which did not show a scaling relationship with distance from, the fault).

Line 336: "They are considered necessary" By whom? Why? This is weak and inexact language.

See reply to comment #2 to this reviewer

Line 348: I have no idea what an "intensive" fracture is.

This has been revised to "high density of" (line 364)

Line 368: depends on your definition of "fault zone" As you point out, this is not an absolute or clearly defined quantity. And what do you mean by "total" fault zone width? Are there other measures of "partial" fault zone width?

Correct, we now state that it is an interpretation of LVZ's (detected by FZGW's) that they are equivalent to fault damage zones, with the relevant studies cited (See line 398)

Line 379: unclear what is meant by "this set"

We have removed this discussion point

Lines 390, 393, 394: more apparent self-contradictions: Is the distance <360 m or is it c. [sic] 500 m? This is VERY confusing. The role of gouge infilling/ or not in these descriptions is not well explained.

The conclusion of this study has been heavily revised to clarify our ideas (lines 424-445). Namely that there is no relationship between proximity to the Alpine Fault and fracture density for distances of <500 m. But, there is a distinct drop off in the density of fractures with a gouge-fill within 160 m of the fault (Figure 7a). This revised manuscript, has also incorporated ideas recently published in Townend et al (2017) based on wireline logs collected during the second phase of the Deep Fault Drilling Project (DFDP-2). Here they present a hierarchical model for the structure of the Alpine Fault, in which the <160 m wide zone of a high density of gouge-filled fracture represents an "inner damage zone" and is surrounded by wider (1-2 km?) zone of open foliation parallel fractures. (Lines 435-445).

Line 397: "development of fault wedges" is a vague physical "explanation" for the occurrence for a spatial zone of gouge-filled fracturing. This interpretation has not been well explained or justified.

See reply to comment #2 to this reviewer

Fig. 1. I disagree that "all active onshore faults" are depicted in this figure. The heavy black line (road) is not labelled or explained, and it is shown far too bold, in my opinion. The road should not be the most conspicuous line feature on this map (but is), in fact it should probably not be shown at all. Why is the transport route even relevant? Lettering/font in the key is too small to be legible.

This should have been correctly stated as showing the faults from the New Zealand Active Fault database (Langridge et al 2016). However, on reflection given that part (a) is an inset, it is quite difficult to see these all these faults, nor do they provide critical information. In the revised figure, we only show the major continental faults on the South Island of New Zealand (i.e. the Alpine Fault and Marlborough Faults).

The road is labelled in part (b). However, we agree that it is given undue prominence, and its weighting has been reduced. State Highway 6 forms a useful reference in this (unpopulated) region and its inclusion is justified. Lettering will be clearer for a full quality version of this image included in a final publication.

Fig. 2. Location of image in part a) is not stated.

This sample was taken from Gaunt Creek, and this information will be included in a revised manuscript.

Fig. 5. Yellow symbols in c) are faint and hard to read. Same for purple symbols in d) and red symbols in a). Symbols are illegibly tiny and the lettering in the key are too small.

Yellow samples in (a) are now red and lettering in key has been enlarged. Note too that the final version of the manuscript will have significantly higher quality images.

Fig. 6. Where were the samples in a, b, and c collected? What intervals? OK I now see this is stated at the bottom of the caption (It makes more sense to cite the interval for parts a, b, c as part of the caption for parts, respectively. This is more efficient. Caption for c should say "In this sample [of what rock type?], fractures show a preference to be aligned: : :"

Sample locations now stated at the start of the caption (Lines 963-964). We have also specified that the rock type in all parts are ultramylonites (Line 961).

Fig. 7. Pole symbols and lettering in b are too small.

The size of the pole symbols in Figure 7b has been increased. The lettering size is of sufficient size in full quality versions of this figure.

Fig. 8. This caption is disorganized, inexact, and confusing. The photos are of limited use at the scale they are presented and they lack adequate labelling and discussion. What are the yellow arrows pointing to? The features in each photo should be labelled on the figure and sequentially and individually discussed and in the caption. What is the scale of g)? e) is almost unreadably muddy. The caption should identify what particular samples were chosen for the CT scans in the lower row of images (parts c, f, and i) and how these 3 chosen CT scans may relate to any of the other samples or field photos in this figure.

The purpose of this figure is to depict the three main types of fractures (separated into columns) noted from field observations and DFDP-1 core. We have revised this figure and its caption to reflect this. We have also added yellow arrows to parts (a), (b) and (e) to specify the fractures we wish to highlight. Arrows in part (6) have also been modified as they show shear sense, not fractures. How the fractures in the field reflect CT scans is noted on line 982.

Fig. 9 "Coincident with lithological diversity" is inexact and physically nonsensical. How can something coincide with a "diversity" Do you mean a contact? I can't see any :gouge filled fractures" in part

"Coincident with lithological diversity" has been revised to "changes in fracture density at lithological contacts" (line 9965). In a revised version of the figure (part d) we have included an additional part which shows gouge-filled fractures in part c.

Reviewer Number 2

This short and concise manuscript describes fractures in the hangingwall of the Alpine fault. It is very well written and illustrated (assuming that the quality of the real images is much better than the ones in the pdf), and contains some useful data. One of the conclusions about the width of the damage zone and how it is defined is well supported by the data.

#1 One question concerns the attribution of the open fractures to low confining pressures. It is argued that the type of fracture varies independently of rock type and therefore that confining pressure must be an additional variable. However, there are other factors that can affect fracture styles, most notably pore fluid pressure. The presence of an open fracture alone does not mean that it formed under low confining pressures (though it is quite possible).

The hypothesis that fractures are kept open by the high pore fluid pressures around the Alpine Fault is an interesting idea; not least as the DFDP-2B boreholes demonstrated that these fractures do transmit fluids (Townend et al 2017). If such a zone existed though, then it would be anticipated that it would be encompassed within the Low Velocity Zone (LVZ) around the Alpine Fault and be detected by FZGW, since pressurised fluids can strongly attenuate seismic velocities (e.g. Nur and Simmons 1969, Jones and Nur 1984, Christensen 1989, Eberhart-Phillips et al 1995). However, this is not the case as the Alpine Fault LVZ is reported to be 60-200 m width (Eccles et al 2015). Consequently, this network of open fracture cannot have contributed to the LVZ; hence our interpretation that this is a near-surface phenomena (Line 417). See also comment #1 by reviewer #1

#2 This discussion highlights a related issue: what are the kinematics of the fractures? This is one area of weakness in the descriptions. Presumably the gouge filled fractures have a shear displacement, but how much and in what directions? What about the open fractures? Do they have any fractographic features giving information on the fracture type? What do the variety of orientations of the gouge filled fractures mean for paleostress? What is their relation to seismicity? Could the differences between the fractures be simply that the open fractures are mode I and the gouge-filled, othermodes? Would this necessarily imply lower pressures?

The omission of information regarding the kinematics of these fractures has now been added (Lines 372-385). In summary, we show that reverse offset is most frequently noted across these fractures (Figure 8f). which is comparable to previous field studies (Cooper and Norris 1994, Norris and Cooper 1997) and descriptions of DFDP-1 core (Toy et al 2015). Furthermore, these studies observe fractures with normal and strike-slip shear sense.

These observations thus indicate that these fractures exhibit a range of shear-senses. This may be linked to the complex interaction between the transpressional strain accommodated across the Alpine Fault and the near-surface topographic stresses (Norris and Cooper 1995, Upton et al 2017; Lines 381-385). Furthermore, it is quite possible that these fractures formed under a dynamic co-seismic stress state that is quite different to the background static state (see also comment #2 by reviewer #1, lines 387-392).

Consequently, though we recognise the value of using gouge-filled fracture orientations to obtain paleostresses orientations around the Alpine Fault, we consider that the range of fracture orientations, shear senses, and a stress state, which varies both spatially and temporally, would preclude such analysis.

With regards to the open fractures, no evidence of shear across them is observed. This supports the idea that they truly represent extensional Mode I fractures and can be termed joints. However, given that foliation, not stress, likely governs their orientation (see comment #1 by reviewer #1, line 429), these also cannot be used as paleostress indicators.

No doubt some of these questions are answered elsewhere or in the process of being answered, but they are relevant to this manuscript. In general it would, however, be good to have a more description of the fractures.

The scan line methodology needs some further justification in the light of recent literature about the circular scan line technique.

We concede that circular scan lines are a superior way of quantitatively assessing fracturing at the outcrop scale (as well document in Watkins et al 2015), however, the outcrops across our stream transects did not lend themselves to this strategy for the following reasons:

1.) *All transects were across (sub) vertical cliff faces. Therefore, if undertaking a circular scan line, the maximum diameter would be 2-3 m as it is limited by the height with which one could accurately measure fracture orientations and fill from a cliff face. By contrasts, a <20 m long scanline along the cliffs base (see Figure below) would contain far more information.*

2.) *The cliff faces are themselves covered in debris or highly friable rock. However, the very base of the cliffs are "cleaned" when the streams are in flood, and so still provide good quality exposure (See Figure S2). Consequently, a long scan-line along the cliff bases will provide the best information on the fracturing at these outcrops.*

These points are now included at lines 168-171. In future, we recognise that quantitative analysis of fracturing may be improved by 3D photogrammetry models or FracPraQ software (Healy et al 2017; n.b. this work flow was not published until after we conducted our fieldwork in 2015-16).

Comments line by line

Line 189-190: Is this valid? What is the relationship between these faults and the Alpine fault? What is they are also part of the damage zone?

We consider these faults to be representative of regional deformation in the Alpine Faults hanging-wall (discussed at Lines 362-365), not the Alpine Fault damage zone per se (as also addressed at for reviewer 1's comments for lines 269-274 and 379). Although clearly the crust is highly deformed for km's into the Alpine Fault 's hanging-wall (as one would expect for the crust next to a plate boundary fault!!), the density of these structures is particularly high only within 160 m of the fault and that is what we consider represents the damage zone (or inner damage zone as defined in Townend et al 2018).

Line 204: Was there any way to check on the validity of these results e.g. compare some nearby surface orientations?

Yes, the orientation of foliation, joints and fractures were subsequently measured in the Amethsyt Tunnel itself (Savage 2013), which was completed after the boreholes, and are broadly consistent with our results (i.e. foliation dips SSE, and fractures and faults are parallel to it). This is now stated at lines 255-257.

Line 230: Is this corrected

These measurements have been corrected for orientation bias, and this has been clarified in the revised manuscript (line 320).

Line 308: How is the confining pressure at which the fractures formed determined?

We apologise that our writing was unclear, this was only meant to be in a qualitative sense. The evidence for this interpretation is discussed in our replies to comment # 1 by reviewer 1 and comment #1 by this reviewer.

Figure 4: I hope that the quality of these images is better than the ones in the pdf, which are so poor that the fractures are entirely unconvincing.

As noted for other comments, the original version of this figure has a much higher resolution, and this will presumably the case at the final publication state.

References

Ampuero, J. P., & Mao, X. (2017). Upper limit on damage zone thickness controlled by seismogenic depth. *Fault Zone Dynamic Processes: Evolution of Fault Properties During Seismic Rupture*, *227*, 243.

Barth, N. C., Toy, V. G., Langridge, R. M., & Norris, R. J. (2012). Scale dependence of oblique plate-boundary partitioning: New insights from LiDAR, central Alpine fault, New Zealand. *Lithosphere*, *4*(5), 435-448.

Barth, N. C., Boulton, C., Carpenter, B. M., Batt, G. E., & Toy, V. G. (2013). Slip localization on the southern Alpine fault, New Zealand. *Tectonics*, *32*(3), 620-640.

Boese, C. M., Townend, J., Smith, E., & Stern, T. (2012). Microseismicity and stress in the vicinity of the Alpine Fault, central Southern Alps, New Zealand. *Journal of Geophysical Research: Solid Earth*, *117*(B2).

Cappa, F., Perrin, C., Manighetti, I., & Delor, E. (2014). Off-fault long-term damage: A condition to account for generic, triangular earthquake slip profiles. *Geochemistry, Geophysics, Geosystems*, *15*(4), 1476-1493.

Chamberlain, C. J., Boese, C. M., & Townend, J. (2017). Cross-correlation-based detection and characterisation of microseismicity adjacent to the locked, late-interseismic Alpine Fault, South Westland, New Zealand. *Earth and Planetary Science Letters*, *457*, 63-72.

Christensen, N. I. (1989). Pore pressure, seismic velocities, and crustal structure. *Geological Society of America Memoirs*, *172*, 783-798.

Cochran, E. S., Li, Y. G., Shearer, P. M., Barbot, S., Fialko, Y., & Vidale, J. E. (2009). Seismic and geodetic evidence for extensive, long-lived fault damage zones. *Geology*, *37*(4), 315-318.

Cooper, A.F., Norris, R.J.,(1994). Anatomy, structural evolution, and slip rate of a plate- boundary thrust: the Alpine fault at Gaunt Creek, Westland. New Zeal. Geol. Soc. Am. Bull. 106, 627-633.

Donath, F. A. (1961). Experimental study of shear failure in anisotropic rocks. *Geological Society of America Bulletin*, *72*(6), 985-989.

Eberhart-Phillips, D., Stanley, W. D., Rodriguez, B. D., & Lutter, W. J. (1995). Surface seismic and electrical methods to detect fluids related to faulting. *Journal of Geophysical Research: Solid Earth*, *100*(B7), 12919-12936.

Eccles, J. D., Gulley, A. K., Malin, P. E., Boese, C. M., Townend, J., & Sutherland, R. (2015). Fault zone guided wave generation on the locked, late interseismic Alpine Fault, New Zealand. *Geophysical Research Letters*, *42*(14), 5736-5743.

Ellsworth, W. L., & Malin, P. E. (2011). Deep rock damage in the San Andreas Fault revealed by P-and S-type fault-zone-guided waves. *Geological Society, London, Special Publications*, *359*(1), 39-53.

Engelder, T. (1985). Loading paths to joint propagation during a tectonic cycle: an example from the Appalachian Plateau, USA. *Journal of Structural Geology*, *7*(3), 459-476.

Healy, D., Rizzo, R. E., Cornwell, D. G., Farrell, N. J., Watkins, H., Timms, N. E., ... & Smith, M. (2017). FracPaQ: A MATLAB™ toolbox for the quantification of fracture patterns. *Journal of Structural Geology*, *95*, 1-16.

Geotech Consulting Limited: Amethyst Hydro Scheme Drilling Investigation Summary 630 Report., 2006

Huang, Y., Ampuero, J. P., & Helmberger, D. V. (2014). Earthquake ruptures modulated by waves in damaged fault zones. *Journal of Geophysical Research: Solid Earth*, *119*(4), 3133-3154.

Jones, T. D., & Nur, A. (1984). The nature of seismic reflections from deep crustal fault zones. *Journal of Geophysical Research: Solid Earth*, *89*(B5), 3153-3171.

Langridge, R. M., Ries, W. F., Farrier, T., Barth, N. C., Khajavi, N., & De Pascale, G. P. (2014). Developing sub 5-m LiDAR DEMs for forested sections of the Alpine and Hope faults, South Island, New Zealand: Implications for structural interpretations. *Journal of Structural Geology*, *64*, 53-66.

Langridge, R. M., Ries, W. F., Litchfield, N. J., Villamor, P., Van Dissen, R. J., Barrell, D. J. A., ... & Lee, J. M. (2016). The New Zealand active faults database. *New Zealand Journal of Geology and Geophysics*, *59*(1), 86-96.

Ma, S., & Beroza, G. C. (2008). Rupture dynamics on a bimaterial interface for dipping faults. *Bulletin of the Seismological Society of America*, *98*(4), 1642-1658.

Mitchell, T. M., & Faulkner, D. R. (2009). The nature and origin of off-fault damage surrounding strike-slip fault zones with a wide range of displacements: a field study from the Atacama fault system, northern Chile. *Journal of Structural Geology*, *31*(8), 802-816.

Mitchell, T. M., & Faulkner, D. R. (2012). Towards quantifying the matrix permeability of fault damage zones in low porosity rocks. *Earth and Planetary Science Letters*, *339*, 24-31.

Norris, R. J., & Cooper, A. F. (2007). The Alpine Fault, New Zealand: surface geology and field relationships. *A Continental Plate Boundary: Tectonics at South Island, New Zealand*, 157-175.

Nasseri, M. H. B., Rao, K. S., & Ramamurthy, T. (2003). Anisotropic strength and deformational behavior of Himalayan schists. *International Journal of Rock Mechanics and Mining Sciences*, *40*(1), 3-23.

Norris, R. J., & Cooper, A. F. (1995). Origin of small-scale segmentation and transpressional thrusting along the Alpine fault, New Zealand. *Geological Society of America Bulletin*, *107*(2), 231-240.

Norris, R. J., & Cooper, A. F. (1997). Erosional control on the structural evolution of a transpressional thrust complex on the Alpine Fault, New Zealand. *Journal of Structural Geology*, *19*(10), 1323-1342.

Nur, A., & Simmons, G. (1969). The effect of saturation on velocity in low porosity rocks. *Earth and Planetary Science Letters*, *7*(2), 183-193.

Perrin, C., Manighetti, I., Ampuero, J. P., Cappa, F., & Gaudemer, Y. (2016). Location of largest earthquake slip and fast rupture controlled by along-strike change in fault structural maturity due to fault growth. *Journal of Geophysical Research: Solid Earth*, *121*(5), 3666-3685.

Paterson, M. S., & Wong, T. F. (2005). Experimental rock deformation-the brittle field. *Springer Science & Business Media.*

Priest, S. D. (1993). Discontinuity analysis for rock engineering. *Springer Science & Business Media.*

Upton, P., Song, B. R., & Koons, P. O. (2017). Topographic control on shallow fault structure and strain partitioning near Whataroa, New Zealand demonstrates weak Alpine Fault. *New Zealand Journal of Geology and Geophysics*, 1-8.

Savage, E. (2013). Investigating Rock Mass Conditions and Implications for Tunnelling and Construction of the Amethyst Hydro Project, Harihari.

Sibson, R. H., White, S. H., & Atkinson, B. K. (1981). Structure and distribution of fault rocks in the Alpine Fault Zone, New Zealand. *Geological Society, London, Special Publications*, *9*(1), 197-210.

Simpson, G. D., Cooper, A. F., & Norris, R. J. (1994). Late quaternary evolution of the Alpine fault zone at Paringa, South Westland, New Zealand. *New Zealand journal of geology and geophysics*, *37*(1), 49-58.

Stern, T., Okaya, D., Kleffmann, S., Scherwath, M., Henrys, S., & Davey, F. (2007). Geophysical exploration and dynamics of the Alpine fault zone. *A Continental Plate Boundary: Tectonics at South Island, New Zealand*, 207-233.

Sutherland, R., Eberhart-Phillips, D., Harris, R. A., Stern, T., Beavan, J., Ellis, S., ... & Townend, J. (2007). Do great earthquakes occur on the Alpine fault in central South Island, New Zealand?. *A continental plate boundary: tectonics at South Island, New Zealand*, 235-251.

Townend, J., Sutherland, R., Toy, V. G., Eccles, J. D., Boulton, C., Cox, S. C., & McNamara, D. (2013). Late-interseismic state of a continental plate-bounding fault: Petrophysical results from DFDP-1 wireline logging and core analysis, Alpine Fault, New Zealand. *Geochemistry, Geophysics, Geosystems*, *14*(9), 3801-3820.

Townend, J., Sutherland, R., Toy, V. G., Doan, M. L., Célérier, B., Massiot, C, et al. (2017). Petrophysical, Geochemical, and Hydrological Evidence for Extensive Fracture-Mediated Fluid and Heat Transport in the Alpine Fault's Hanging-Wall Damage Zone. *Geochemistry, Geophysics, Geosystems. 18(12), 4709-4732*

Toy, V. G., Boulton, C. J., Sutherland, R., Townend, J., Norris, R. J., Little, T. A., ... & Scott, H. (2015). Fault rock lithologies and architecture of the central Alpine fault, New Zealand, revealed by DFDP-1 drilling. *Lithosphere*, *7*(2), 155-173.

Toy, V. G., Sutherland, R., Townend, J., Allen, M. J., Becroft, L., Boles, A., ... & Daube, C. (2017). Bedrock geology of DFDP-2B, central Alpine Fault, New Zealand. New Zealand Journal of Geology and Geophysics, 60(4), 497-518.

Watkins, H., Bond, C. E., Healy, D., & Butler, R. W. (2015). Appraisal of fracture sampling methods and a new workflow to characterise heterogeneous fracture networks at outcrop. *Journal of Structural Geology*, *72*, 67-82.

Weng, H., Yang, H., Zhang, Z., & Chen, X. (2016). Earthquake rupture extents and coseismic slips promoted by damaged fault zones. *Journal of Geophysical Research: Solid Earth*, *121*(6), 4446-4457.

Williams, J. N., Toy, V. G., Massiot, C., McNamara, D. D., & Wang, T. (2016). Damaged beyond repair? Characterising the damage zone of a fault late in its interseismic cycle, the Alpine Fault, New Zealand. *Journal of Structural Geology*, *90*, 76-94.

Williams, J. N., Toy, V. G., Smith, S. A., & Boulton, C. (2017). Fracturing, fluid-rock interaction and mineralisation during the seismic cycle along the Alpine Fault. *Journal of Structural Geology*, *103*, 151-166.

Controls on fault zone structure and brittle fracturing in the foliated hanging-wall of the Alpine Fault

Jack N. Williams[a]*, Virginia G. Toy[a], Cécile Massiot[b,c], David D. McNamara[c,d], Steven A. F. Smith[a], Steven Mills[e]

Affiliations:

[a]Department of Geology, University of Otago, PO Box 56, Dunedin 9054, New Zealand

[b]School of Geography, Environment, and Earth Sciences, Victoria University of Wellington, PO Box 600, Wellington 6012, New Zealand

[c]GNS Science, PO Box 30-368, Lower Hutt 5040, New Zealand

[d]Department of Earth and Ocean Sciences, NUI Galway, University Road, Galway, Ireland

[e]Department of Computer Science, University of Otago, PO Box 56, Dunedin 9054, New Zealand

*Corresponding Author:** Jack Williams, now at: School of Earth and Ocean Sciences, Cardiff University, Cardiff, CF10 3AT, United Kingdom (email: williamsj132@cardiff.ac.uk)

Abstract

Three datasets are used to quantify fracture density, orientation, and fill in the foliated hanging-wall of the Alpine Fault: (1) X-ray computed tomography (CT) images of drill-core collected within 25 m of its principal slip zones (PSZs) during the first phase of the Deep Fault Drilling Project that were reoriented with respect to borehole televiewer images, (2) field measurements from creek sections up to 500 m from the PSZs, and (3) CT images of oriented drill-core collected during the Amethyst Hydro Project at distances of ~0.7-2 km

Deleted: [e]

Deleted: [d]

Moved (insertion) [2]

Deleted: [e]

Deleted:

Deleted: [d]

Moved up [2]: [d]Department of Earth and Ocean Sciences, NUI Galway, University Road, Galway, Ireland

Deleted: [a]

Deleted: jack.williams@otago.ac.nz

Formatted: Default Paragraph Font

Deleted: The orientations and densities of fractures in the foliated hanging-wall of the Alpine Fault provide insights into the role of a mechanical anisotropy in upper crustal deformation, and the extent to which existing models of fault zone structure can be applied to active plate-boundary faults.

Deleted: were

Deleted: damage

Deleted: at different distances from the principal slip zones (PSZs) of the Alpine Fault

Deleted: principal slip zones (PSZs)

Deleted: the

Deleted: at

Deleted: <

Deleted: 500-1400

Deleted: m

from the PSZs. Results show that within 160 m of the PSZs in foliated cataclasites and ultramylonites, gouge-filled fractures exhibit a wide range of orientations. At these distances, fractures are interpreted to have formed at relatively high confining pressures and/or in rocks that had a weak mechanical anisotropy. Conversely, at distances greater than 160 m from the PSZs, fractures are typically open and subparallel to the mylonitic or schistose foliation, implying that fracturing occurred at low confining pressures and/or in rocks that were mechanically anisotropic. Fracture density is similar across the ~500 m width of the field transects. By combining our datasets with measurements of hydraulic conductivity and seismic velocity around the Alpine Fault, we further develop the hierarchical model for hanging-wall damage structure that was proposed by Townend et al., (2017). The wider zone of foliation-parallel fractures represents an 'outer damage zone' that forms in the near-surface. The distinct <160 m wide interval of widely oriented gouge-filled fractures constitutes an 'inner damage zone.' This zone is interpreted to extend to the base of the seismogenic crust given that its width is comparable to: (1) the Alpine Fault low-velocity zone detected by fault zone guided waves, and (2) damage zones reported from other exhumed large-displacement faults. In summary, a narrow zone of fracturing at the base of the Alpine Fault's hanging-wall seismogenic crust is anticipated to widen in the near-surface, which is consistent with fault zone flower structure models.

Deleted: relatively

Deleted: had

Deleted: or schistosity

Deleted: were

Deleted: of the hanging-wall datasets

Deleted: the

Deleted: damage

Deleted: (

Deleted: open

Deleted: forms

Deleted: e

Deleted: widthof the inner damage zone is

Deleted: to

Deleted: e width

Deleted: other large-displacement

Deleted: crust

Deleted: , indicating that the Alpine Fault does not have a typical "damage zone" defined by decreasing fracture density with distance. Instead, we conclude that the ~160 m-wide zone of intensive gouge-filled fractures provides the best estimate for the width of brittle fault-related damage. This estimate is similar to the 60-200 m wide Alpine Fault low-velocity zone detected through fault zone guided waves, indicating that a majority of its brittle damage occurs within its hanging-wall rather than the footwall.

Keywords: fractures, anisotropy, Alpine Fault, Deep Fault Drilling Project, damage zone

1. Introduction

Conceptual models of fault zone structure in the upper crust often invoke a relatively narrow "fault core" that accommodates most displacement, surrounded by a halo of heavily fractured rock termed the "damage zone" (Caine et al., 1996; Chester et al., 1993; Chester and Logan, 1986; Faulkner et al., 2010). These models have been successfully applied in a variety of tectonic settings and for a wide range of fault displacements and exhumation depths (e.g. Choi et al., 2016; Faulkner et al., 2010; Kim et al., 2004; Mitchell and Faulkner, 2009;

Savage and Brodsky, 2011). However, the term "damage zone" has been applied by geologists and geophysicists to describe a variety of fault-related features, such as fractures and faults at stepovers and bends (Chester and Chester, 2000; Kim et al., 2004; Mitchell and Faulkner, 2009; Wilson et al., 2003), the volume of inelastic deformation that is induced by dynamic stresses during earthquake rupture propagation (Andrews, 2005; Cowie and Scholz, 1992; Rice et al., 2005; Templeton et al., 2008; Vermilye and Scholz, 1998), and the volume of rock in which earthquake swarms or foreshock and aftershock sequences are localised (Kim and Sanderson, 2008; Savage et al., 2017; Sibson, 1989; Yukutake et al., 2011). Furthermore, though damage zones are typically reported to be <1 km wide (Faulkner et al., 2011; Savage and Brodsky, 2011), co-seismic ground shaking can modify fracture permeability many hundreds of kilometres away from the fault source (Cox et al., 2015; Muir-Wood and King, 1993; O'Brien et al., 2016).

Brittle faults often develop in mylonite sequences or other (e.g. jointed) rocks that contain compositional and mechanical anisotropies (Bistacchi et al., 2012; Chester and Fletcher, 1997; Massironi et al., 2011). Evidence from field studies (Bistacchi et al., 2010; Peacock and Sanderson, 1992), experiments (Donath, 1961; Misra et al., 2015; Paterson and Wong, 2005), and numerical modelling (Chester and Fletcher, 1997) demonstrates that such anisotropy can significantly affect the orientation and density of brittle fractures. Despite this, "fault core-damage zone" models are based largely on field observations from relatively isotropic host rocks, and there have been comparatively few field studies (Bistacchi et al., (2010) being a notable exception) that document the influence of mechanical anisotropy on patterns of brittle fracture damage in large-displacement faults.

In this contribution, multiple datasets across a range of scales were used to analyse fracture densities, orientations, and mineral fills across the hanging-wall of the Alpine Fault's central section. Measurements from within 25 m of the Alpine Fault principal slip zones (PSZs) were

Deleted: range

Deleted: in a fairly inconsistent way (Choi et al., 2016; Cochran et al., 2009; Peacock et al., 2016). TFor example, the term "damage zone" has been used to describe

Deleted: as well as

Deleted: 5

Deleted: at distances of

Deleted: and homogenous

made from shallow (depths <130 m) drill-cores and wireline logs obtained during the first phase of the Deep Fault Drilling Project (DFDP-1). These are combined with field studies at distances <500 m from the PSZs and analyses of drill-core recovered at 0.7-2.0 km from the PSZs during the Amethyst Hydro Project (AHP). Results are then compared to measurements of hydraulic conductivity (Cox et al., 2015; Townend et al., 2017) and geophysical studies (Boese et al., 2012; Chamberlain et al., 2017; Eccles et al., 2015) around the Alpine Fault. In doing so, we critically assess the application of "damage zone" models to a plate-boundary-scale structure. Furthermore, the Alpine Fault is an active fault that rapidly exhumes ductile-to-brittle fault rock sequences from depths of up to 35 km (Little et al., 2005; Norris and Toy, 2014). Fracturing in its hanging-wall therefore overprints a 1-2 km wide mylonite sequence containing a pervasive foliation (Cooper and Norris, 1994; Norris and Cooper, 1997, 2007; Toy, 2008), and so can provide new insights into the relationships between fracturing and mechanical anisotropy.

2. Tectonic setting of the Alpine Fault

The Alpine Fault is a crustal-scale (along strike extent ~850 km, depth ~35 km) transpressive discontinuity accommodating ~70% of Pacific-Australian plate motion in the South Island of New Zealand (DeMets et al., 1994; Norris and Cooper, 2001, Figure 1a). This study focuses on the central section between the Toharoa and Martyr Rivers (Barth et al., 2013) where it currently accommodates dextral strike-slip at a rate of 27 ± 5 mm/yr and dip-slip at a rate of 6-10 mm/yr (Little et al., 2005; Norris and Cooper, 2001).

In the central section at depths greater than 8-12 km, the Alpine Fault accommodates motion via viscous creep across a >1 km wide ductile shear zone in which the hanging-wall "Alpine Schist" protolith is progressively mylonitised (Norris and Cooper, 2007; Toy et al., 2010).

Deleted: we present a comprehensive study of fracture densities, orientations, and mineral fills across the hanging-wall of the Alpine Fault' central section.

Deleted: In addition, t

Deleted: Brittle f

Deleted: sub-parallel to the main fault surface

Deleted: provides an opportunity to assess the influence of rock anisotropy on brittle fracturing. Observations of fracturing were made from multiple datasets and across a range of scales. Measurements from within 25 m of the Alpine Fault principal slip zones (PSZs) were made from shallow (depths <130 m) drill-cores and wireline logs obtained during the first phase of the Deep Fault Drilling Project (DFDP-1). These are combined with field studies at distances <500 m from the PSZs and analyses of drill-core recovered at 500-1400 m from the PSZs during the Amethyst Hydro Project (AHP). Results are then compared to measurements of hydraulic conductivity (Cox et al., 2015; Townend et al., 2017) and geophysical studies (Boese et al., 2012; Chamberlain et al., 2017; Eccles et al., 2015) to improve our understanding of the structure of the Alpine Fault and to provide

Deleted: It can be potentially divided along-strike into five sectionsSlip rates vary along strike such that it can be broadly divided into three sections: (1) a northern section between Lake Rotoiti and its intersection with the Hope Fault near Hokitika, (2) a central section between Hokitika and Haast (Figure 1a), and (3) a southern section between Haast and its offshore termination near the Puysegur subduction zone (Barth et al., 2013; Norris and Cooper, 2007; Sutherland et al., 2007).

Deleted: the fault

Deleted:

Shear strains increase with proximity to the Alpine Fault and are recorded by protomylonites, mylonites and ultramylonites, which occur in spatial sequence towards the fault (Figure 2; Norris and Cooper, 2003; Reed, 1964; Toy et al., 2008). Foliation in the mylonite sequence is mainly defined by alternating quartzofeldspathic and mica-rich layers (Figure 2). Bottle-green hornblende-rich metabasic mylonites, and purple-dark grey mylonites that are comparatively mica rich are also present. Their presence reflects variations in protolith lithology (Cooper and Norris, 2011; Norris and Cooper, 2007; Sibson et al., 1981; Toy, 2008). As the mylonites in the hanging-wall are exhumed to depths of less than 8-12 km, temperatures drop below those at which quartz plasticity occurs and brittle structures start to overprint the mylonitic shear zone (Norris and Cooper, 2007; Toy et al., 2010, 2015). This brittle overprint is reflected in the formation of a ~20 m thick layer of green, indurated and often foliated cataclasite (Allen et al., 2017; Toy et al., 2015), and a 10-50 cm thick clay-rich PSZ that is preserved adjacent to the currently-active fault trace (Boulton et al., 2017, 2012; Ikari et al., 2014; Mitchell and Toy, 2014).

To the first-order (i.e. at scales >10 km), the trace of the Alpine Fault is remarkably linear, with an average strike of 055º (Norris and Cooper, 2007). On the basis of geophysical imaging and measurements of the mylonitic foliation -which is thought to parallel the fault- it is estimated to dip at ~45º in its central section (Sibson et al., 1981; Stern et al., 2007), though this may locally exceed 60º (Little et al., 2005; Toy et al., 2017). At scales of 1-10 km, perturbations in the regional stress field induced by hanging-wall topography results in segmentation of the Alpine Fault. Segmentation is rooted to depths of 0.5-4 km and comprises km-long, approximately E-W striking and steeply-dipping strike-slip fault strands, which adjoin NE-SW striking, gently-dipping (~30º) thrust segments (Barth et al., 2012; Langridge et al., 2014; Norris and Cooper, 1995, 2007; Simpson et al., 1994; Upton et al., 2017).

Deleted: ,
Deleted: so that aand form a sequence of
Deleted: which
Deleted: is
Deleted: ultramylonite
Deleted: s
Deleted: occur in
Deleted: ing
Deleted: form
Deleted:), which
Deleted: are exhumed to the surface in the Alpine Fault's hanging-wall
Deleted: (
Deleted: These are then exhumed to the surface in the Alpine Fault's hanging-wall.
Deleted: layers
Deleted: and
Deleted: ,
Deleted: or
Deleted: ,
Deleted: , and
Deleted: s
Deleted: s
Deleted: s are exhumed
Deleted: structures
Deleted: principal slip zone (
Deleted:)
Deleted: ... [1]
Deleted: r structure
Deleted: and which, o
Deleted: measurements
Deleted: ,,
Deleted: and geophysical imaging
Deleted: (Toy et al., 2017) indicate that at depths >4 km the central section of the Alpine Fault zone can be considered a single sub-planar structure, which is thought to have the same orientation as the regional mylonitic foliation (055/45 SE).
Deleted: However
Deleted: , at depths of less than 0.5-4 km
Deleted: f
Deleted: trace
Deleted: This s
Deleted: c.,form into a series of s
Deleted:
Deleted:
Deleted: and
Deleted: that extend to depths of 0.5-4 km

3. Methods

3.1 Fracture orientations from DFDP-1 drill-core

Hanging-wall fracture orientations immediately adjacent to the Alpine Fault's PSZ were assessed through analysis of datasets arising from the first phase of the Deep Fault Drilling Project (DFDP-1, http://alpine.icdp-online.org). DFDP-1 successfully sampled the Alpine Fault in two boreholes (DFDP-1A and DFDP-1B, Figure 3) at depths of less than 150 m at Gaunt Creek (Figure 1b, Sutherland et al., 2012). The geophysical properties of the DFDP-1 boreholes were characterised by a full suite of wireline logs (Townend et al., 2013). These were combined with visual descriptions of ~70 m of core recovered across the two boreholes to construct a lithological classification scheme for DFDP-1 drill-core (Figure 3, Toy et al., 2015).

Abundant fractures were observed in X-ray computed tomography (CT) scans of DFDP-1 drill-core (Williams et al., 2016). The true orientations of these fracture were obtained by generating 'unrolled' CT images of individual core sections (Mills and Williams, 2017), which are directly analogous to geographically referenced - but lower resolution - borehole televiewer (BHTV) images. Where fractures could be matched between the two images, a rotation could be derived to transform all fracture orientations in the CT scans from a local core reference frame to their true geographic orientation (Figure 4). Depending on the number of fractures matched, core was rotated with a high, moderate, or low degree of confidence. In DFDP-1A, the quality of BHTV imaging was insufficient to attempt matching fractures, whereas in the Alpine Fault's relatively intact footwall (Townend et al., 2013), too few fractures (<1 fracture/core-section) could be imaged to attempt core reorientation. Therefore, the true orientation of fractures was only determined for the depth interval 94-126 m in the DFDP-1B borehole (Figure 3). Given the orientation of PSZ-1 (which separates hanging-wall and footwall cataclasite) sampled in DFDP-1 (015/43 E; Townend et al., 2013), this spans an

Deleted: ology

Deleted: at less than 25 m orthogonal distance from the

Deleted: in early 2011

Deleted: , which

Deleted: core

Deleted: , typically with a gouge-fill,

Deleted: The true orientation of these fractures was determined for the depth interval 94-126 m in the DFDP-1B borehole (Figure 3).

Deleted: T

Deleted: orientations

Deleted: >

Deleted: (

orthogonal distance of ~25 m. A full methodology is provided in Appendix A, the rotations applied to DFDP-1 core sections are listed in Table S1, and a complete CT-BHTV image comparison is given in Williams et al (2017b).

3.2 Field observations of fracture orientations and densities

At orthogonal distances of up to 150-250 m from the PSZs, fracture orientations and densities were measured in four creeks (Gaunt Creek, Stony Creek, Hare Mare Creek and Havelock Creek, Figure 1b) that cut across the hanging-wall sequence approximately perpendicular to the main fault trace (Figure S1). Along each creek, fracture orientations and densities were measured at 3 or 4 stations. This information was also gathered from approximately 500 m from the Alpine Fault at Bullock Creek (Figure 1b). Each creek transect cuts across a thrust segment of the Alpine Fault, so the orthogonal distance between the measuring stations and the PSZs was calculated assuming a fault dip of 30º (Norris and Cooper, 1995, 1997). The mylonite lithology for each station was classified using the scheme presented by Toy (2008).

The outcrops encountered along these transects are typically sub-vertical and may be covered by debris except at their bases where they are frequently cleaned by flood events (Figure S2). They are therefore poorly-suited for fracture density analysis using circular scanlines (e.g. Mauldon et al., 2001). Instead, the fracture density was calculated from the number and orientation of fractures that intersected a linear transect along the base of each outcrop (Priest, 1993; Schulz and Evans, 2000). This technique has the tendency to under-sample fractures oriented at low angles to the scan-line. Therefore, a weighting (*w*) factor calculated using a modified version of the Terzaghi correction (Massiot et al., 2015; Terzaghi, 1965) was applied to each fracture, and results are shown as 'corrected' fracture density.

Deleted: ,

Deleted: mylonite

Deleted: collected

Deleted: Additional information was also collected

Deleted: at

Deleted: around

Deleted: c.

Deleted: in

Deleted: so the

Deleted: by

Deleted: ,

Deleted: s

Deleted: . I

Deleted: , the fracture density

Deleted: T

Deleted: e density of fractures at each measuring station was calculated following the methodology of Hudson and Priest, (1983) and Schulz and Evans, (2000),

Deleted: where the

Deleted:

Deleted: was recorded

3.3 Fracture orientations in the Amethyst Hydro Project boreholes

Deleted: and densities

The Amethyst Hydro Project (AHP) was developed to divert water from the Amethyst Ravine down a 1040 m-long tunnel to a powerhouse on the floodplain of the Wanganui River. Prior to the main phase of tunnelling, four exploratory boreholes (BH1-4; Figure 1b and S3) were completed between 2005-2006, resulting in the recovery of ~890 m of drill-core at depths of 50-200 m. The boreholes are situated 1-2 km southeast of a thrust segment of the Alpine Fault, where it may conceivably dip at a range of 30-60º (Norris and Cooper, 1995; Toy et al., 2017). The drill-cores are therefore at orthogonal distances of ~0.7-2.0 km from the PSZs.

Deleted: 2

Deleted: of a total

Deleted: the surface trace of the

Deleted: 45

Deleted: . Below the boreholes, the Alpine Fault dips c. 45º to the east

Deleted: meaning that drill-cores are

Deleted: 5

Deleted: 1.7

Deleted: 4

To provide a dataset analogous to the DFDP-1 CT scans, a total of 31.9 m of drill-core from the AHP boreholes was CT scanned at the Southern Cross Hospital in Wellington, New Zealand. Initial descriptions of the drill-core found that the Rock Quality Designation (RQD, the % of intact core lengths >100 mm/1 m of drill-core) varied considerably due to intense fracturing adjacent to the Tarpot Fault and other minor faults that intersect the AHP boreholes (Geotech Consulting Limited, 2006; Savage, 2013). However, for practical reasons scanning was focussed on intervals of high RQD (Figure S3). The CT scanner was operated at 100 mA and an X-ray tube voltage of 120 kVp. Slice spacing was 1.25 mm, field of view 250 mm, and the image size was 512 x 512 pixels. Therefore, the size of one voxel is 0.488 x 0.488 x 1.25 mm in the x, y, z directions respectively. Reconstruction of two-dimensional CT slices into three-dimensional images of the drill-core was performed using OsiriX Imaging Software (http://www.osirix-viewer.com/).

Deleted: . Intervals with RQD values less than 10% are related to intense

Deleted: , Figure S3

Deleted: To ensure that the description of the fracture network sampled in the AHP is unaffected by damage from these minor faults, CT

Deleted: 2

AHP drill-core was not oriented. However, the orientation of the schistosity is noted in the drill-core logs to an accuracy of ±5° (Geotech Consulting Limited, 2006), where it is consistent with the schistosity orientation measured in the Amethyst Tunnel itself (Savage, 2013). It can thus be used as a reference to reorient drill-core CT scans back into a geographic

Deleted: prominent

Deleted: observed in the

Deleted: s has a known orientation

Deleted: and

reference frame. For BH2 and BH3 drill-cores, which are vertical, this required only a single transformation. For the inclined BH1 and BH4 drill-cores, this required first rotating the core with respect to the foliation. These orientations were then corrected for the inclination of the drill core using the Planes from Oriented and Navigated Drillcore (POND) Excel spreadsheet (Stanley and Hooper, 2003).

3.4 Statistical analysis of fracture orientations

The clustering intensity of fracture orientations was quantified using the resultant vector method of Priest, (1993), where the vector for each fracture was weighted by the Terzaghi correction for misorientation bias (Massiot et al., 2015; Terzaghi, 1965). This analysis was performed only for the DFDP-1 and AHP datasets, which sampled a large population (>100) of fractures. Field measuring stations sampled too few (<30) fractures to reliably perform this analysis, and so their clustering is described in a qualitative sense only.

4. Results

4.1 Fracture orientations in DFDP-1 drill-core within 25 m of the Alpine Fault

In the DFDP-1 CT images, a total of 637 fractures were rotated into their true geographic orientation where they show a weak cluster about the orientation of the foliation and Alpine Fault PSZs at Gaunt Creek (015/43 E, Figures 5a, Appendix B; Townend et al., 2013). Features in DFDP-1B BHTV images are also aligned about this orientation, but with a higher cluster intensity than fractures noted in the CT images (Figure 5b, Table 1). This may reflect: (1) features observed at the resolution of the BHTV are more likely to be aligned subparallel to the fault plane and foliation than those visible in CT, and/or (2) some of the planar features identified from the BHTV images were the mylonitic foliation itself. The clustering of fractures hosted in foliated ultramylonites and cataclasites (Units 1, 2 and 4 of Toy et al., 2015) is the same as fractures hosted in relatively homogenous unfoliated cataclasites (Unit 3

Formatted: Heading 2

Deleted: .

Deleted: Thus, we describe clustering of fractures measured at field stations at field stationsin a qualitative sense only

Deleted: (Figure 5a; Appendix B). In both the CT and BHTV datasets, a set of fractures is observed sub-parallel to the mylonitic

Deleted: orientation

Deleted: and b

Deleted: Features,

Deleted: Clustering of this fracture set is stronger in the lower-resolution BHTV images indicating that

Deleted: fractures

Deleted: structures

Deleted: The comparison between CT and BHTV images is discussed further in Appendix B.

Deleted: ... [2]

Deleted: No clear relationships are generally observed between the type of fracture-fill (Table 1 of Williams et al., 2016) and fracture orientation (Figure 5a). Plotted separately in Figures 5c and 5d are

Deleted: f

Deleted: and

of Toy et al., 2015; Figures 5c and d, Table 1). We also observed no clear relationships between fracture fill (Table 1 of Williams et al., 2016) and fracture orientation (Figure 5a).

4.2 Fracture orientations, densities, and fill in field transects within 500 m of the Alpine Fault

The orientations and densities of fractures observed in the four field transects are summarised in Figure 7. In these transects, similar fractures to those observed in the CT scans of DFDP-1 core are identified (Figure 8). Total fracture density in the transects varies between 3-30 fractures/metre, and there is no clear decrease in fracture density with increasing distance from the Alpine Fault in any of the transects (Figure 7a). Gouge-filled fractures (Figure 8a-c) are observed at all distances from the Alpine Fault but are relatively abundant (>1 fracture/metre, Figure 7a, Table S2) within 100-160 m of the PSZs (Figure 7a). The thicker gouge-filled fractures (>1 cm) commonly juxtapose different lithologies or offset markers (Figure 8d-f). Thinner gouge-filled fractures (<1 cm) are localised within 160 m of the Alpine Fault. Open fractures (Figure 8g-i) are present at all stations, though are most prevalent at those furthest from the fault (Figure 7b).

The composition of the mylonites can also affect fracture density. When they are juxtaposed together, micaceous mylonites and ultramylonites are observed to contain relatively high densities of gouge-filled fractures compared to quartzofeldspathic mylonites and ultramylonites (Figures 9a and b). Localities that showed the widest range in fracture orientations tend to be less than 160 m from the PSZs within the ultramylonites (Figure 7b). Within mylonite units, fracture orientations tend to be more aligned to the foliation (Figure 7b), although gouge-filled fractures can sometimes cut across it (e.g. Bullock Creek).

Deleted: It is evident that fractures in the foliated units are more clustered around the local Alpine Fault and foliation orientation than fractures in the homogenous units. However, even within the foliated units there are many fractures that cut across the foliation at a wide range of orientations (Figure 5c and 6).

Deleted: -

Deleted: r-main

Deleted: structures

Deleted: are

Deleted: s

Deleted: Distinctive g

Deleted: Fault, but

Deleted: only

Deleted: within

Deleted: approximately

Deleted:

Deleted: g

Deleted: i

Deleted: 1

Deleted: d

Deleted: f

Deleted: Intervals of micaceous

Deleted: when they are juxtaposed against

Deleted: At Hare Mare Creek station 2, the disappearance of thin gouge-filled fractures coincides with a transition from micaceous-quartzofeldspathic mylonite to quartzofeldspathic mylonites (Figure 9c).

Deleted: a

Deleted: a

Deleted: , Figure 7b

4.3 Fractures in AHP drill-core, 0.7-2.0 km from the Alpine Fault

The AHP sampled grey, well-foliated Alpine Schist (Figure 10), a subgroup of the Haast Schist (textural zone III-IV, Turnbull et al., (2001); Cox and Barrell., (2007)). Fracture orientations are clustered about the orientation of the host rock schistosity in agreement with the findings during initial drill-core descriptions and observations within the Amethyst Tunnel itself (Figure 11; Geotech Consulting Limited, 2006; Savage, 2013). The clustering of these fracture orientations is stronger than in the DFDP-1 datasets (Table 1). Fractures that cut across the schistosity are most frequent in BH4 (Figure 10d and 11).

Though fractures are predominantly open, it is conceivable that the original fill may have been lost during the subsequent core handling processes. This means that standard schemes to differentiate between natural and induced fractures (Kulander et al., 1990; Williams et al., 2016) cannot be applied to this dataset. Nevertheless, some open fractures must be natural as they show alteration haloes (Figure 10a) implying that they were once conduits for fluid-flow. Furthermore, packer tests conducted in these boreholes indicate hydraulic conductivities of ~10^{-6}-10^{-5} ms^{-1}, which is equivalent to permeabilities of 10^{-13}-10^{-12} m^2 (Cox et al., 2015; Geotech Consulting Limited, 2006). No permeability measurements have been made in the schist protolith at greater distances from Alpine Fault, however, these measurements are orders of magnitude higher than has been reported in other metamorphic rock terranes (~10^{-20}-10^{-17} m^2; Manning and Ingebritsen, 1999) and for typical continental crust (~10^{-17} m^2; Townend and Zoback, 2000).

5 Discussion

5.1 Fracture orientations in anisotropic wall rocks in the Alpine Fault hanging-wall

Two styles of fracturing are evident in the foliated Alpine Fault cataclasite, mylonite and schist sequence (Figure 12). Within DFDP-1 drill-core, fractures are predominantly gouge-

Deleted: 500-1400 m
Deleted: 1.7
Deleted: schist bedrock of the
Deleted: Group
Deleted: generally aligned. Foliation is defined by alternating quartzo-feldspathic and micaceous layers (Figure 10a and b). All 239 fractures measured in the CT scans of drill-core are plotted in Figure 11. There is a strong alignment
Deleted: of fractures
Deleted: o t
Deleted: and the regional Alpine Fault orientation,
Deleted: ,
Deleted: Furthermore, t
Deleted:
Deleted: Therefore, we can only note qualitatively that fracture density appears to be strongly controlled by the presence of gouge-filled faults (Figure S3) as has also been previously documented (Geotech Consulting Limited, 2006; Savage, 2013). We also find that
Deleted: open
Deleted: , implying that they are natural and were once conduits for fluid-flow.
Deleted:
Deleted: mechanic
Deleted: ally anisotropic

filled and exhibit a range of orientations (Figure 5 and 6) with only a small proportion (11%) of fractures in foliated cataclasites and ultramylonites clearly foliation-parallel (Williams et al., 2016). However, in schists sampled by the AHP drill-core, the fractures are more clustered about the foliation than in DFDP-1 drill-core (Figure 11, Table 1). The difference in fracture clustering between the DFDP-1 and AHP drill-cores is qualitatively replicated by the field transects, where fractures show variable orientations immediately adjacent to the Alpine Fault but are typically foliation-parallel at the sites furthest from the fault (Figure 7). Furthermore, field transects show that the variably oriented fractures have a gouge-fill, whilst foliation-parallel fractures further from the fault tend to be open (Figures 7 and 8).

Experimental studies on foliated rocks demonstrate that mechanical anisotropy will exert the greatest control on rock failure when: (1) the angle between the maximum principal stress σ_1 and the anisotropy (α) is ~30º, (2) confining pressure is low (<35 MPa), and (3) the mechanical 'strength' of the anisotropy is high (Donath, 1961; Misra et al., 2015; Nasseri et al., 2003; Paterson and Wong, 2005). The first factor can be approximated for the Alpine Fault given the mylonite's average orientation of 055/45SE (Norris and Cooper, 2007) and the stress tensor orientation within the surrounding crust, determined from focal mechanisms of microseismicity in the fault's hanging-wall (Boese et al., 2012). This yields a value of α of approximately 44º, when measured in the plane containing the maximum and minimum principal stresses. This can be considered an intermediate value of α, since in deformation experiments fractures may form parallel or non-parallel to the foliation depending on the combination of confining pressure and lithology (Donath, 1961; Nasseri et al., 2003; Paterson and Wong, 2005).

Foliation-parallel fractures are least common in the ultramylonites and foliated cataclasites. Indeed, in the DFDP-1 datasets, there is no difference in fracture clustering between foliated and unfoliated units (Table 1). Lithology may control mechanical anisotropy depending on

Deleted: However, in

Deleted: host rock

Deleted: round

Deleted: predominantly foliation-parallel

Deleted: in

Deleted: In

Deleted:

Deleted: clustered

Deleted: parallel

Deleted: , open, foliation-parallel fractures are found at all localities, but they are most common at distances greater than 160 m from the Alpine Fault in the mylonite and protomylonite sequence (Figure 7). Overall, there is a transition from dominantly open, foliation-parallel fractures at distances greater than 160 m from the PSZs, to gouge-filled fractures with more variable orientations closer to the fault (Figure 12).

Deleted: Alpine Fault

Deleted: (σ_1 and σ_3)

Deleted: generally

mineralogy, porosity, grain size, and the nature of the foliation surfaces (Donath, 1961; Nasseri et al., 2003). It is notable that phase mixing and grain size reduction in the ultramylonites reduces the intensity of the foliation, compared to the relatively coarse-grained schists, protomylonites, and mylonites (Figure 2; Norris and Cooper, 2007; Toy et al., 2010, 2008). These data suggest that this lithological change could have a marked effect on the orientation of fractures. Compositional variations between relatively quartzofeldspathic and relatively micaceous mylonites can also influence the density of fractures (Figure 9). These observations highlight that fracturing in the upper crust may be influenced by lithological variations developed within an underlying linked, and synkinematic, shear zone. However, at other localities (e.g. Stony Creek, Figure 7), variations in dominant fracture characteristics are confined within units of similar composition and texture. This suggests that variations in confining pressure may also be important in controlling the relationship between fractures and foliation, as discussed in the next section.

5.2 Fracture damage around the Alpine Fault

Field transects across the Alpine Fault's hanging-wall show that fracture density remains roughly constant (>3.5 fractures/m, corrected for orientation bias) for at least 500 m from the fault (Figure 7a). Furthermore, the AHP (Cox et al., 2015) and DFDP-2B boreholes (Sutherland et al., 2017; Townend et al., 2017) demonstrate an interval of enhanced permeability (10^{-16}-10^{-13} m^2) that extends for at least 2 km into the Alpine Fault's hanging-wall. Permeability in this rock mass is controlled by open fractures (Cox et al., 2015; Sutherland et al., 2017; Townend et al., 2017) that are generally foliation-parallel (Massiot, 2017), and so directly analogous to the fractures sampled in the field (Figure 8g-i) and in AHP drill-core (Figure 10). Conventional definitions of fault structure, that use fracture density and permeability as criteria for damage zone width (e.g. Berg and Skar, 2005; Caine et al., 1996; Faulkner et al., 2010; Savage and Brodsky, 2011; Schulz and Evans, 2000),

Deleted: (Figure 2a)

Deleted: b

Deleted:) (

Deleted: is

Deleted: suggest

Deleted:

Deleted: ing

Deleted: foliation-parallel

Deleted: in some cases

Deleted: For example, at Hare Mare Creek, there is a sharp lithological boundary between micaceous and quartzofeldspathic mylonite, and gouge-filled fractures predominate in the former, while open foliation-parallel fractures predominate in the latter (Figure 9c).

Deleted: imposed by

Deleted: ... [3]

Deleted: indicates

Deleted: are

Deleted: with foliation-parallel fractures forming at relatively low confining pressures compared to fractures adjacent to the Alpine Fault in the ultramylonites. Indeed, it is likely foliation-parallel fractures formed as confining pressure was released (Engelder, 1985; Price, 1959; Zangerl et al., 2006) during rapid exhumation (6-9 mm/yr) of the hanging-wall along the Alpine Fault (Little et al., 2005; Tippett and Kamp, 1995).

Deleted: Caine et al., (1996) defined a fault damage zone as "a network of subsidiary structures that bound the fault core and may enhance fault zone permeability relative to the core and undeformed protolith." In applying this definition, most previous work has defined the damage zone as a volume of rock that shows elevated fracture densities compared to a "background" level of fracturing that normally includes widely-spaced regional fracture or joint sets (e.g. Berg and Skar, 2005; Faulkner et al., 2010; Savage and Brodsky, 2011; Schulz and Evans, 2000). Our data from the field

Deleted: of

Deleted: into the hanging-wall

Deleted: at distances 200-1500 m from the Alpine Fault an active hydrogeological system was sampled by the DFDP-2B borehole (Sutherland et al., 2017; Townend et al., 2018).

would therefore suggest that the Alpine Fault's damage zone extends for at least 500 m, and possibly 2 km, into its hanging-wall.

Nevertheless, within the field transects we also note a distinct interval adjacent to the Alpine Fault's PSZs that contains a relatively high density of gouge-filled fractures (>1 fracture/metre, Figure 7a). The width of this interval is <147 m (i.e. station 4) from the PSZs at Gaunt Creek, <103 m at Stony Creek (i.e. station 3), <151 m at Hare Mare Creek (at station 2, Figure 8c) and <160 m at Havelock Creek (i.e. stations 4). These width estimates are based on assumption that the Alpine Fault dips at 30° below the measuring stations (see the methods section). However, the fault dip may locally vary (for example, the fault dip sampled by DFDP-1 was 43°; Townend et al., (2013)), and there is also uncertainty in the depth extent of its near-surface segmentation (Barth et al., 2012; Norris and Cooper, 1995; Upton et al., 2017). Nevertheless, even if the fault dipped at 45° (Norris and Cooper, 2007) beneath the measuring stations, the zone of higher-density gouge-filled fractures would be <205 m wide (Table S3) and so is still appreciably closer to the Alpine Fault than the intervals sampled by the AHP and DFDP-2 boreholes.

It is this ~100-160 m wide interval with a high density of gouge-filled fractures that Norris and Cooper (1997, 2007) interpreted as the extent Alpine Fault's central section hanging-wall damage zone. Furthermore, the width of this zone is comparable to damage zones widths estimated elsewhere on the Alpine Fault (e.g. Barth et al., 2013 along the southern section; Wright, 1998 at the northern end of the the central section, Figure 13a) and to other crustal-scale fault zones that have accommodated hundreds of kilometres of displacement (Figure 13b; Faulkner et al., 2011; Savage and Brodsky, 2011).

Deleted: This zone may therefore extend for distances of at least 1-2 km from the Alpine Fault

Deleted: km-scale around the Alpine Fault,

Deleted: ,

Deleted: we also note a Despite these observations, we suggest that the damage zone surrounding the Alpine Fault is most appropriately represented by the localised zone that

Deleted: s

Deleted: (

Deleted: and 8

Deleted: an

Deleted: thezoneer

Deleted: <

Deleted: (i.e. station 4)

Deleted: ... [4]

Deleted: (

Deleted: higher-density

Deleted: as measured at Havelock Creek) and is <170 m in all other localities (

Deleted: .

Deleted: ,

Deleted: (Figure 13b), rapidly-moving (~few cm/yr)

Deleted: (Biegel and Sammis, 2004; Childs et al., 2009; Finzi et al., 2009; Manighetti et al., 2007; Perrin et al., 2016; Savage and Brodsky, 2011; Savage and Cooke, 2010).

Interpretations of damage zone width within the Alpine Fault's hanging-wall may therefore differ by an order of magnitude depending on what criteria is used. To reconcile this, Townend et al., (2017) suggested that the ~2 km wide interval of enhanced permeability and foliation-parallel fracturing can be considered as an 'outer damage zone' (Figure 12). Fractures within this zone may have formed by co-seismic shaking and slip on critically-stressed fractures (Cox et al., 2015; Townend et al., 2017), or by the release of confining pressure (Engelder, 1985; Price, 1959; Zangerl et al., 2006) during rapid exhumation (6-9 mm/yr) of the hanging-wall (Little et al., 2005; Tippett and Kamp, 1995). Rare gouge-filled fractures (<1 fracture/metre) in this interval (e.g. Figure 8e) may also be the structures accommodating the diffuse, low to moderate magnitude (M_W <6) seismicity that has been recorded in a ~5 km wide zone within the Alpine Fault's hanging-wall (Boese et al., 2012; Chamberlain et al., 2017; Eberhart-Phillips, 1995).

Conversely, the <160 m wide zone with a relatively high density of gouge-filled fractures defines a narrower 'inner damage zone' (Figure 12; Townend et al. 2017). Microstructural and compositional analysis of these fractures indicates that they formed in response to wear and shearing of the wall rock and were subsequently mineralised due to circulation of hydrothermal fluids (Warr and Cox, 2001; Williams et al., 2017a). Offset markers across gouge-filled fractures (particularly those <1 cm thick) are rarely observed in DFDP-1 core and field transects, but where they are present, reverse offset is most frequently noted (Figure 8d; Norris and Cooper, 1997; Toy et al., 2015). "Gouge-filled shears" that accommodated strike-slip (Norris and Cooper, 1997), normal dip-slip (Cooper and Norris, 1994), or a combination of both (Barth et al., 2012) have also been observed.

Cooper and Norris, (1994) interpreted that dip-slip fractures facilitated imbrication, tectonic thickening and rotation of Alpine Fault thrust sheets as they moved across the irregular topography of the footwall gravels. Dextral shears are interpreted to reflect the partitioning of

Deleted: ring
Deleted: may
Deleted: define
Deleted: .
Deleted: along
Deleted: filled
Deleted: with silicate mineralisation from
Deleted: fractures that accommodated normal
Deleted:
Deleted: or that are s and contain s have also been(Norris and Cooper, 1997).
Deleted: *(Barth et al 2012)*
Formatted: Font:Italic
Deleted: (
Deleted: *Cooper and Norris (1995)*
Deleted: these
Deleted: it

strike-slip movement away from shallowly dipping PSZs (Barth et al., 2012). The diverse range of fracture orientations and shear senses in gouge-filled fractures therefore indicates complex internal deformation of Alpine Fault thrust sheets in the near-surface (<500 m), as they facilitate transpressional motion under the influence of km scale along-strike variations in stress induced by the topography (Norris and Cooper, 1995; Upton et al., 2017).

Fractures may have also formed due to dynamic off-fault stresses (Ma, 2009; Rice et al., 2005) during M_W >7.5 Alpine Fault earthquake ruptures (Sutherland et al., 2007). The relatively thin seismogenic crust in the Alpine Fault's hanging-wall (10 ± 2 km, Boese et al., (2012)) will limit the generation of dynamic co-seismic damage to within ~100-200 m of the fault (Ampuero and Mao, 2017). To the first order, this is comparable to the width of the inner damage zone reported here.

5.3 Comparison to geophysical data

A 60-200 m wide low-velocity zone (LVZ) that extends to depths of ~8 km has been documented around the Alpine Fault from the detection and character of Fault Zone Guided Waves (FZGWs; Eccles et al., 2015). FZGWs are commonly regarded as an *in situ* indicator of fault damage zone width (Ben-Zion and Sammis, 2003; Eberhart-Phillips et al., 1995; Ellsworth and Malin, 2011; Li et al., 2014). Given the comparable widths of the Alpine Fault LVZ (60-200 m) and the inner damage zone described here (100-160 m), we speculate that the inner damage zone may trap FZGWs in the Alpine Fault hanging-wall. If this is true, it implies that the inner damage zone extends to depths of ~8 km, consistent with the relatively high-temperature (<400 °C) mineralising phases (calcite and chlorite) present in the gouge-filled fractures (Williams et al., 2017a).

Deleted:

Deleted: (*Barth et al 2012).*

Deleted: . This complexity is likely driven by a combination of facilitating transpressional motional and the

Deleted: They are considered necessary to the development of near-surface (<4 km) fault wedges that facilitate complex oblique-slip Alpine Fault movement (Barth et al., 2012; Norris and Cooper, 1997).

Deleted: Incremental shear f

Deleted: have formed due to imposition of

Deleted: They may also reflect the

Deleted: during

Deleted: , when the hanging-wall would bewould be in compression in the case ofin the case of up-dip rupture propagation (Ma and Beroza, 2008; Rice et al., 2005).

Deleted: (

Deleted: can

Deleted: depth range over are able to

Deleted:

Deleted: Gouge-filled fractures are present at all distances in our field transects (Figure 7-9) and within the AHP drill-core (Figure 10c). However, their interval of high density (>1 fracture/metre) is restricted to less than 118-147 m from the PSZs at Gaunt Creek (i.e. between stations 3-4), <73-103 m at Stony Creek (i.e. between stations 2-3), <151 m at Hare Mare Creek (at station 2, Figure 8c) and <154-160 m at Havelock Creek (i.e. between stations 3-4). This is consistent with the observations of Norris and Cooper, (2007) who suggested that the Alpine Fault's central section damage zone can be defined by a ~100 m wide zone of intensive gouge-filled fractures. These estimates of damage zone width are also similar to those made elsewhere on the Alpine Fault (e.g. Barth et al., 2013 in the southern section in South Westland; Wright, 1998 at the northern end of the the central section, Figure 13a) and to other predictions for crustal-scale (Figure 13b), rapidly-moving (~few cm/yr) fault zones that have accommodated hundreds of kilometres of displacement (Biegel and Sammis, 2004; Childs et al., 2009; Finzi e ... [5]

Deleted: A relatively narrow (<100-160 m) hanging-wall damage zone is also broadly consistent with the presence of a

Deleted: L

Deleted:

Deleted: V

Deleted: Z

Deleted: around the Alpine Fault

Deleted: and character

Deleted: (

Deleted: This was detected by Fault Zone Guided Waves (FZGWs)

Deleted: that

Deleted: the width of the

Deleted: zone

Deleted: e.g. give example of clay and temperature estimate here;

Though the boundary between the mylonites and ultramylonites is also ~100 m from the Alpine Fault (Norris and Cooper, 2003; Toy et al., 2008), these two units have roughly similar seismic velocities (Adam et al., 2016; Allen et al., 2017; Christensen and Okaya, 2007) and so are unlikely to channel FZGWs. We also note that since FZGWs are an indicator of total fault zone width, our interpretation implies that most of the Alpine Fault's LVZ is located in its hanging-wall. Western Province basement rocks to the west of the Alpine Fault are rarely exposed (Lund Snee et al., 2014; Norris and Cooper, 2007), and so it remains unknown if its footwall damage zone is indeed relatively narrow.

That the FZGWs are not being channelled by the margins of the ~2 km wide outer damage zone leads us to conclude that this is a near-surface feature only (i.e. fractures are not kept open at depth by pressurised fluids). If correct, this model of the Alpine Fault's hanging-wall structure conforms to the expectations of fault zone flower structure models, which predict a narrow inner damage zone that extends through the seismogenic crust, surrounded by a wider zone of fractures in the near-surface at low confining pressures (~<3 km, Figure 12; e.g. Finzi et al., 2009; Sylvester, 1988).

6. Conclusions

Fracture orientations and densities in the foliated hanging-wall of the Alpine Fault's central section were quantified in drill-core from the Deep Fault Drilling Project (DFDP-1), field transects in four creek sections, and drill-core recovered from the Amethyst Hydro Project. At distances greater than approximately 160 m from the Alpine Fault principal slip zones (PSZs), open and foliation-parallel fractures dominate. These are interpreted to form at low confining pressures in mechanically anisotropic schist and mylonites. At distances less than ~160 m from the PSZs, gouge-filled fractures with a wide range of orientations predominate. Fracture density and orientation are locally influenced by changes in host rock lithology, but overall

- **Deleted:** Alpine Fault
- **Deleted:** ... [6]
- **Deleted:**
- **Deleted:** t
- **Deleted:** 1-
- **Deleted:** instead
- **Deleted:** If the FZGWs are sampling the zone of intensive gouge-filled fracturing, it therefore indicates that the >500 m wide interval of open foliation-parallel fractures are a near-surface feature only. This is consistent with our interpretation that these fractures formed at low confining pressures during exhumation within the Alpine Fault's hanging wall.
- **Deleted:** s
- **Deleted:** and that is
- **Deleted:**)
- **Deleted:** (
- **Deleted:**
- **Deleted:** Pervasive minor faults have been mapped for distances of tens of kilometres from the Alpine Fault (Cox and Barrell, 2007; Cox and Sutherland, 2007). We interpret that the occasional (<1 fracture/metre) gouge-filled fractures observed herein AHP drill-core and in the field at distances greater than 160 m from the Alpine Fault (e.g. Figure 8e) are equivalent to this set. These fractures may also be the exhumed equivalent of structures that are currently accommodating the diffuse, low-moderate magnitude (M_W <6) seismicity that has been recorded at depths less than 10 km in the Alpine Fault's hanging-wall (Boese et al., 2012; Chamberlain et al., 2017; Eberhart - Phillips, 1995).
- **Deleted:** Alpine S
- **Deleted:** s
- **Deleted:** Alpine Fault
- **Deleted:** that are mechanically anisotropic
- **Deleted:** c.

fracture density is approximately constant at distances of up to ~500 m from the PSZs (Figure 12).

Following Townend et al., (2017), we interpret that the ~2 km wide zone of open foliation-parallel fractures within the hanging-wall represents an "outer damage zone" that forms at low confining pressures and relatively shallow depths. Conversely, the 160 m-wide zone of gouge-filled fractures represents an "inner damage zone." The width of this zone is similar to estimates for the low-velocity zone (LVZ) around the Alpine Fault made by Fault Zone Guided Waves. We therefore interpret that the inner damage zone is the geological manifestation of the LVZ, which if true, implies that the inner damage zone also extends to depths of ~8 km. Overall, our interpretations are compatible with a flower structure model for damage in the Alpine Fault's hanging-wall, with a relatively narrow zone of damage extending towards the base of the seismogenic crust, which broadens upwards towards the surface.

Code availability

The code to generate 'unrolled' circumferential CT images is available from the GFZ data service (http://pmd.gfz-potsdam.de/panmetaworks/review/7f1b114f11b67f540bb1360ead692dc578a66e3d0935c7fef6ffe210db285300-icdp/).

Data availability

In the supplementary information, we include detailed field maps and cross sections (Figure S1), photos of outcrops used for quantifying fracture density (Figure S2), a cross section through the Amethyst Tunnel and location of boreholes (Figure S3), and an example of AHP CT scans (Figure S4). The following tables are also provided, a list of rotations applied to DFDP-1B core (Table S1), a summary of field transects (Table S2), and estimates of the

Deleted: c.

Deleted:

Deleted: We interpetconclude that these observations are indicative of flower structure model

Deleted: of fracturing within t the Alpine Fault's hanging-wall, consistent with the model proposed by

Deleted: (

Deleted: *Townend et al (2018)*. O

Deleted: extending xx m into the

Deleted:

Deleted: is most suitably defined by the approximately

Deleted: ,

Deleted: . These fractures formed at relatively high confining pressures and/or in relatively mechanically isotropic ultramylonites and foliated cataclasites. They are interpreted to have been generated during the development of fault wedges and/or the dynamic effect of ruptures propagating along the Alpine Fault. Comparison of our field-based estimates of damage zone width (160 m) to the total thickness of the low-velocity zone measured in geophysical data (60-200 m) suggests that the Alpine Fault damage zone is asymmetric, with most brittle fault-related damage focussed in its hanging-wall.

Deleted: 2

Deleted: 3

Deleted:

Deleted: and

distance of field measuring stations from the Alpine Fault for different fault dips (Table S3). Lithological distribution and Alpine Fault location as per University of Otago fault zone mapping program, which is available at: http://www.otago.ac.nz/geology/research/structural-geology/alpine-fault/af-maps.html. DFDP-1 and AHP CT scan 'core logs' and CT-BHTV image comparison are available on the GFZ data service (http://pmd.gfz-potsdam.de/panmetaworks/review/52b75045a30f1bd60f7fd5b841e69c468885e2a10dfc3704e50b236df2ef8608-icdp).

Acknowledgements

DFDP-1 was funded by: GNS Science; Victoria University of Wellington; the University of Otago; the University of Auckland; the University of Canterbury; Deutsche Forschungsgemeinschaft and the University of Bremen; Natural Environment Research Council grants NE/J024449/1, NE/ G524160/1 and NE/H012486/1 and the University of Liverpool; and the Marsden Fund of the Royal Society of New Zealand. The International Continental Scientific Drilling Program, ICDP (www.icdp-online.org) provided extensive support. JW was supported by a University of Otago Doctoral Scholarship. We thank Matthew Parris at the Oncology Department at Dunedin Hospital, and Darren Tod at the Southern Cross Hospital, Wellington, for support in collecting CT scans of DFDP-1 Amethyst Hydro Project drill-core respectively. Katrina Sauer, Ben Melosh and Astrid Vetrhus provided field assistance. Comments by Tim Little and Tom Blenkinsop, and by two anonymous reviewers on an earlier version of this manuscript, improved this paper.

Deleted: Core

Deleted: i

Appendix A: DFDP-1B core rotation methodology

The technique employed to reorient core DFDP-1 here is similar to that described in Jarrard et al., (2001), Paulsen et al., (2002) and Shigematsu et al., (2014), however, instead of comparing DFDP-1 BHTV data to DMT CoreScan system® unrolled core scans, we compare

BTHV images to 'unrolled' CT core images. The acquisition and interpretation of the DFDP-1 BHTV logs has been previously described by Townend et al., (2013) and McNamara, (2015). DFDP-1 CT scans consist of a stack of core-axial perpendicular image slices with a pixel size of 0.244 mm and a spacing of 1 mm. The CT stack for each core section was loaded into Fiji (http://fiji.sc/Fiji) and a circle was manually defined around the irregular boundary of drill-core in a core axial-perpendicular image slice using the code available at Mills and Williams, (2017). This circle was then used to define the path of the image in all other slices. Generation of the unrolled images accounts for the fact that the spacing between individual CT slices (1 mm, i.e. the core-axial parallel pixel size) is greater than the pixel size within the slices (0.244 mm). Unrolled images were then reflected around the borehole axis as an image of the outer surface of the core and a BHTV image are reflections of each other. This technique has benefits over methods using the DMT CoreScan system®, since drill-core does not have to be physically rotated and so can be used without the risk of damaging fragile core sections.

Unrolled CT images were imported into the composite log viewing software WellCAD® (http://www.alt.lu/wellcad.htm) along with the BHTV images, where they are placed side-by-side to allow matching of structures (Figure 4, see also Williams et al., (2017b)). When correlating the two datasets, it was first necessary to account for possible depth shifts between recorded drill-core depths and BHTV imagery due to factors such as stretching of the logging cable and intervals from which no drill-core was recovered (Haggas et al., 2001; Jarrard et al., 2001). In this study, a depth shift of no more than ±30 cm was allowed.

Deleted: s

Deleted: were

The orientation of fractures in the DFDP-1 CT images had previously been measured within a local core reference frame (see Figure 4 in Williams et al., 2016). Since the DFDP-1 boreholes were vertical, corrections to reorient the drill-core back into a geographic reference frame required only a single rotation about the core axis to correct for the dip direction. When correlating structures, errors may be introduced by: (1) the internal BHTV magnetometer (±2°), (2) the manual picking of sinusoidal curves on BHTV and unrolled CT images that can be ±10° for shallowly dipping (<30°) structures (Jarrard et al., 2001), and (3) the fact that the DFDP-1B BHTV data imaged the open borehole, which has a larger diameter (127 mm) than the drill-core (85 mm). To mitigate against the cumulative effect of these errors, Jarrard et al., (2001) stitched unrolled images of many different core sections together that spanned intervals of 5-30 m, prior to the matching with BHTV imagery. This meant that only a single rotation was necessary for all core sections across the entire stitched interval, which could be based on identifying ~20-30 matching structures between the BHTV and unrolled core images.

In DFDP-1 it was not possible to stitch unrolled CT images of core section together as no prominent reference marker across different sections were identified. Consequently each <1 m long core section had to be reoriented individually, within which we never identified more than 3 matching structures. Therefore, compared to the methodology described by Jarrard et al., (2001), the degree of confidence on the applied reorientation was strongly dependent on the quality of individual matches for each core section and the range of rotations that they indicated. We recorded this qualitatively for each core section using the scheme outlined below.

- High degree of confidence: images matched with one very prominent structure (e.g. Figure 4d), or matched with two or more structures whose range of suggested rotations are within 10° of each other (Figure 4b and c).

- Moderate degree of confidence: images matched with one prominent feature or two features that indicate rotations that range 10-19° (e.g. Figure 4a) or three features whose range of suggested rotations are within 20-30° of each other.

- Low degree of confidence: images matched with one feature or two features whose range of suggested rotations are within 20-30° of each other.

In this scheme, a core reorientation is deemed unreliable if the range of rotations suggested by different structures is ≥30°, i.e. equivalent to the cumulative effect of possible errors listed above. For those core sections where more than one matching structure was identified, the rotation that was applied was derived from the average of that required for each match. If one of the matched structures was more prominent, then the applied rotation was biased towards that structure.

Deleted:

Appendix B: DFDP-1B core rotation validity

Based on the criteria presented in Appendix A, of the 40 core sections from DFDP-1B in which there was suitable quality of unrolled CT and BHTV images to attempt reorientation (Figure 3), 31 were reoriented (Table S1). Prior to reorientation, fractures in these sections exhibit no clustering (Figure A1a), however, a weak one does develop after reorientation (Figure 5a). Since fractures in nature typically exhibit non-random orientations, this is evidence that the reorientation of the CT scans was successful (Kulander et al., 1990; Paulsen et al., 2002). In addition, fractures within some individual core sections (Figure A1b), and fractures rotated based on a high degree of confidence (Figure A1c) contain a wide range of orientations.

The recognition of fractures in unrolled CT images that are not observed in BHTV can be readily explained by the higher resolution of the CT images. However, structures are also observed in the BHTV logs, but not interpreted as fractures in the CT images (Figure 4). This may represent noise in the BHTV images, or in the case of foliation-parallel structures, the ultramylonitic foliation itself since it can be difficult to differentiate these structures. The subordinate north-dipping set of fractures in the BHTV images (Figure 5b) is not recognised in the orientations gathered from CT images (Figure 5a). A similar north dipping fracture set was also recognised in DFDP-2B BHTV images (Massiot 2017), and their causation and relevance is the focus of ongoing work.

Competing Interests

Authors declare that they have no conflict of interest.

References

Adam, L., Toy, V. and Boulton, C.: Mylonites as shales? Experimental observations of P-wave anisotropy dependence on mineralogy, layering and scale, in SEG Technical Program Expanded Abstracts 2016, pp. 3169–3173, Society of Exploration Geophysicists., 2016.

Allen, M. J., Tatham, D., Faulkner, D. R., Mariani, E. and Boulton, C.: Permeability and seismic velocity and their anisotropy across the Alpine Fault, New Zealand: An insight from laboratory measurements on core from the Deep Fault Drilling Project phase 1 (DFDP-1), J. Geophys. Res. Solid Earth, 122(8), 6160–6179, doi:10.1002/2017JB014355, 2017.

Ampuero, J. P. and Mao, X.: Upper limit on damage zone thickness controlled by seismogenic depth, Fault Zo. Dyn. Process. Evol. Fault Prop. Dur. Seism. Rupture, 227, 243, 2017.

Andrews, D. J.: Rupture dynamics with energy loss outside the slip zone, J. Geophys. Res. Solid Earth, 110(1), 1–14, doi:10.1029/2004JB003191, 2005.

Barth, N. C., Toy, V. G., Langridge, R. M. and Norris, R. J.: Scale dependence of oblique plate-boundary partitioning: New insights from LiDAR, central Alpine fault, New Zealand, Lithosphere, 4(5), 435–448, doi:10.1130/L201.1, 2012.

Barth, N. C., Boulton, C., Carpenter, B. M., Batt, G. E. and Toy, V. G.: Slip localization on the southern Alpine Fault New Zealand, Tectonics, 32(3), 620–640, doi:10.1002/tect.20041, 2013.

Ben-Zion, Y. and Sammis, C. G.: Characterization of Fault Zones, Pure Appl. Geophys., 160(3), 677–715, doi:10.1007/PL00012554, 2003.

Berg, S. S. and Skar, T.: Controls on damage zone asymmetry of a normal fault zone: Outcrop analyses of a segment of the Moab fault, SE Utah, J. Struct. Geol., 27(10), 1803–1822, doi:10.1016/j.jsg.2005.04.012, 2005.

Bistacchi, A., Massironi, M. and Menegon, L.: Three-dimensional characterization of a crustal-scale fault zone: The Pusteria and Sprechenstein fault system (Eastern Alps), J. Struct. Geol., 32(12), 2022–2041, doi:10.1016/j.jsg.2010.06.003, 2010.

Bistacchi, A., Massironi, M., Menegon, L., Bolognesi, F. and Donghi, V.: On the nucleation of non-Andersonian faults along phyllosilicate-rich mylonite belts, Geol. Soc. London, Spec. Publ., 367(1), 185–199, doi:10.1144/sp367.13, 2012.

Boese, C. M. M., Townend, J., Smith, E. and Stern, T.: Microseismicity and stress in the vicinity of the Alpine Fault, central Southern Alps, New Zealand, J. Geophys. Res. Solid Earth, 117(2), doi:10.1029/2011JB008460, 2012.

Boulton, C., Yao, L., Faulkner, D. R., Townend, J., Toy, V. G., Sutherland, R., Ma, S. and Shimamoto, T.: High-velocity frictional properties of Alpine Fault rocks: Mechanical data, microstructural analysis, and implications for rupture propagation, J. Struct. Geol., 97, 71–92, doi:10.1016/j.jsg.2017.02.003, 2017.

Boulton, C. J., Carpenter, B. M., Toy, V. and Marone, C.: Physical properties of surface outcrop cataclastic fault rocks, Alpine Fault, New Zealand, Geochemistry, Geophys. Geosystems, 13(1), doi:10.1029/2011GC003872, 2012.

Caine, J. S., Evans, J. P. and Forster, C. B.: Fault zone architecture and permeability structure, Geology, 24(11), 1025–1028, 1996.

Chamberlain, C. J., Boese, C. M. and Townend, J.: Cross-correlation-based detection and characterisation of microseismicity adjacent to the locked, late-interseismic Alpine Fault, South Westland, New Zealand, Earth Planet. Sci. Lett., 457, 63–72, doi:10.1016/j.epsl.2016.09.061, 2017.

Chester, F. M. and Chester, J. S.: Stress and deformation along wavy frictional faults, J. Geophys. Res., 105(B10), 23421, doi:10.1029/2000JB900241, 2000.

Chester, F. M. and Logan, J. M.: Implications for mechanical properties of brittle faults from observations of the Punchbowl fault zone, California, Pure Appl. Geophys. PAGEOPH, 124(1–2), 79–106, doi:10.1007/BF00875720, 1986.

Chester, F. M., Evans, J. P. and Biegel, R. L.: Internal structure and weakening mechanisms of the San Andreas Fault, J. Geophys. Res., 98(B1), 771, doi:10.1029/92JB01866, 1993.

Chester, J. S. and Fletcher, R. C.: Stress distribution and failure in anisotropic rock near a bend on a weak fault, J. Geophys. Res. Earth, 102(B1), 693–708, doi:10.1029/96JB02791, 1997.

Choi, J. H., Edwards, P., Ko, K. and Kim, Y. S.: Definition and classification of fault damage zones: A review and a new methodological approach, Earth-Science Rev., 152, 70–87, doi:10.1016/j.earscirev.2015.11.006, 2016.

Christensen, N. I. and Okaya, D. A.: Compressional and shear wave velocities in South Island, New Zealand rocks and their application to the interpretation of seismological models of the New Zealand crust, A Cont. Plate Bound. Tectonics South Island, New Zeal., 123–155, 2007.

Columbus, J., Sirguey, P. and Tenzer, R.: A free, fully assessed 15-m DEM for New Zealand, Surv. Q., 66(66), 16–19, 2011.

Cooper, A. F. and Norris, R. J.: Anatomy, structural evolution, and slip rate of a plate-boundary thrust: the Alpine Fault at Gaunt Creek, Westland, New Zealand, Geol. Soc. Am. Bull., 106(5), 627–633, doi:10.1130/0016-7606(1994)106<0627:ASEASR>2.3.CO;2, 1994.

Cooper, A. F. and Norris, R. J.: Inverted metamorphic sequences in Alpine fault mylonites produced by oblique shear within a plate boundary fault zone, New Zealand., 2011.

Cowie, P. A. and Scholz, C. H.: Physical Explanation for the Displacement Length Relationship of Faults Using a Post-Yield Fracture-Mechanics Model, J. Struct. Geol., 14(10), 1133–1148, doi:10.1016/0191-8141(92)90065-5, 1992.

Cox, S. C., Menzies, C. D., Sutherland, R., Denys, P. H., Chamberlain, C. and Teagle, D. A. H.: Changes in hot spring temperature and hydrogeology of the Alpine Fault hanging wall, New Zealand, induced by distal South Island earthquakes, Geofluids, 15(1–2), 216–239, 2015.

DeMets, C., Gordon, R. G., Argus, D. F. and Stein, S.: Effect of recent revisions to the geomagnetic reversal time scale on estimate of current plate motions, Geophys. Res. Lett., 21(20), 2191–2194, doi:10.1029/94GL02118, 1994.

Donath, F. A.: Experimental study of shear failure in anisotropic rocks, Geol. Soc. Am. Bull., 72(6), 985–989, doi:10.1130/0016-7606(1961)72[985:ESOSFI]2.0.CO;2, 1961.

Eberhart-Phillips, D., Stanley, W. D., Rodriguez, B. D. and Lutter, W. J.: Surface seismic and electrical methods to detect fluids related to faulting, J. Geophys. Res., 100(B7), 12919–12936, doi:10.1029/94JB03256, 1995.

Eberhart-Phillips, D.: Examination of seismicity in the central Alpine fault region, South Island, New Zealand, New Zeal. J. Geol. Geophys., 38(4), 571–578, 1995.

Eccles, J. D., Gulley, A. K., Malin, P. E., Boese, C. M., Townend, J. and Sutherland, R.: Fault Zone Guided Wave generation on the locked, late interseismic Alpine Fault, New Zealand, Geophys. Res. Lett., 42(14), 5736–5743, doi:10.1002/2015GL064208, 2015.

Ellsworth, W. L. and Malin, P. E.: Deep rock damage in the San Andreas Fault revealed by P- and S-type fault-zone-guided waves, Fagereng, A., Toy, V.G., Rowland, J. (Eds), Geol. Earthq. Source A Vol. Honor Rick Sibson, Geol. Soc. London, Spec. Publ., 359(1), 39–53, doi:10.1144/SP359.3, 2011.

Engelder, T.: Loading paths to joint propagation during a tectonic cycle: an example from the Appalachian Plateau, U.S.A., J. Struct. Geol., 7(3–4), 459–476, doi:10.1016/0191-8141(85)90049-5, 1985.

Faulkner, D. R., Jackson, C. A. L., Lunn, R. J., Schlische, R. W., Shipton, Z. K., Wibberley, C. A. J. and Withjack, M. O.: A review of recent developments concerning the structure, mechanics and fluid flow properties of fault zones, J. Struct. Geol., 32(11), 1557–1575, doi:10.1016/j.jsg.2010.06.009, 2010.

Faulkner, D. R., Mitchell, T. M., Jensen, E. and Cembrano, J.: Scaling of fault damage zones with displacement and the implications for fault growth processes, J. Geophys. Res. Solid Earth, 116(5), doi:10.1029/2010JB007788, 2011.

Finzi, Y., Hearn, E. H., Ben-Zion, Y. and Lyakhovsky, V.: Structural properties and deformation patterns of evolving strike-slip faults: Numerical simulations incorporating damage rheology, Pure Appl. Geophys., 166(10–11), 1537–1573, doi:10.1007/s00024-009-0522-1, 2009.

Geotech Consulting Limited: Amethyst Hydro Scheme Drilling Investigation Summary Report., 2006.

Haggas, S., Brewer, T. S., Harvey, P. K. and Iturrino, G. I.: Relocating and orientating cores by the integration of electrical and optical images, J. Geol. Soc. London, 158, 615–623, doi:10.1144/jgs.158.4.615, 2001.

Ikari, M. J., Carpenter, B. M., Kopf, A. J. and Marone, C.: Frictional strength, rate-dependence, and healing in DFDP-1 borehole samples from the Alpine Fault, New Zealand, Tectonophysics, 630(C), 1–8, doi:10.1016/j.tecto.2014.05.005, 2014.

Jarrard, R. D., Paulsen, T. S. and Wilson, T. J.: Orientation of CRP-3 core, Victoria Land Basin, Antarctica, Terra Antarct., 8(3), 161–166, 2001.

Kim, Y. S. and Sanderson, D. J.: Fault propagation, displacement and damage zones, Struct. Geol. New Res., 1, 99–117, 2008.

Kim, Y. S., Peacock, D. C. P. and Sanderson, D. J.: Fault damage zones, J. Struct. Geol., 26(3), 503–517, doi:10.1016/j.jsg.2003.08.002, 2004.

Kulander, B. R., Dean, S. L. and Ward, B. J.: Fracture core analysis: interpretation, logging and use of natural and induced fractures in core, American Association of Petroleum Geologists., 1990.

Langridge, R. M., Ries, W. F., Farrier, T., Barth, N. C., Khajavi, N. and De Pascale, G. P.: Developing sub 5-m LiDAR DEMs for forested sections of the Alpine and Hope faults, South Island, New Zealand: Implications for structural interpretations, J. Struct. Geol., 64, 53–66, doi:10.1016/j.jsg.2013.11.007, 2014.

Lees, J. M.: RFOC: Graphics for spherical distributions and earthquake focal mechanisms. R package version 3.3-3. http://CRAN.R-project.org/package=RFOC, R Packag. version, 3(2), 2014.

Li, Y. G., De Pascale, G. P., Quigley, M. C. and Gravley, D. M.: Fault damage zones of the M7.1 Darfield and M6.3 Christchurch earthquakes characterized by fault-zone trapped waves, Tectonophysics, 618, 79–101, doi:10.1016/j.tecto.2014.01.029, 2014.

Little, T. A., Cox, S., Vry, J. K. and Batt, G.: Variations in exhumation level and uplift rate along the obliqu-slip Alpine fault, central Southern Alps, New Zealand, Geol. Soc. Am. Bull., 117(5), 707, doi:10.1130/B25500.1, 2005.

Lund Snee, J. E., Toy, V. G. and Gessner, K.: Significance of brittle deformation in the footwall of the Alpine Fault, New Zealand: Smithy Creek Fault zone, J. Struct. Geol., 64, 79–98, doi:10.1016/j.jsg.2013.06.002, 2014.

Ma, S.: Distinct asymmetry in rupture-induced inelastic strain across dipping faults: An off-fault yielding model, Geophys. Res. Lett., 36(20), doi:10.1029/2009GL040666, 2009.

Manning, C. E. and Ingebritsen, S. E.: Permeability of the continental crust: Implications of geothermal data and metamorphic systems, Rev. Geophys., 37(1), 127–150, doi:10.1029/1998RG900002, 1999.

Massiot, C.: Fracture system characterisation and implications for fluid flow in volcanic and metamorphic rocks, , 1–191, 2017.

Massiot, C., Mcnamara, D. D. and Lewis, B.: Geothermics Processing and analysis of high temperature geothermal acoustic borehole image logs in the Taupo Volcanic Zone , New Zealand, Geothermics, 53, 190–201, doi:10.1016/j.geothermics.2014.05.010, 2015.

Massironi, M., Bistacchi, A. and Menegon, L.: Misoriented faults in exhumed metamorphic complexes: Rule or exception?, Earth Planet. Sci. Lett., 307(1–2), 233–239, doi:10.1016/j.epsl.2011.04.041, 2011.

Mauldon, M., Dunne, W. M. and Rohrbaugh, M. B.: Circular scanlines and circular windows: New tools for characterizing the geometry of fracture traces, J. Struct. Geol., 23(2–3), 247–258, doi:10.1016/S0191-8141(00)00094-8, 2001.

McNamara, D.: Exploring New Zealand's subsurface using borehole images, in Presented at the 2015 New Zealand Geosciences Conference, Wellington, 25-27th November (2015)., 2015.

Mills, S. and Williams, J. N.: Generating circumferential images of tomographic drill-core scans, GFZ Data Serv., doi:http://doi.org/10.5880/ICDP.5052.005, 2017.

Misra, S., Ellis, S. and Mandal, N.: Fault damage zones in mechanically layered rocks: The effects of planar anisotropy, J. Geophys. Res. B Solid Earth, 120(8), 5432–5452, doi:10.1002/2014JB011780, 2015.

Mitchell, T. M. and Faulkner, D. R.: The nature and origin of off-fault damage surrounding strike-slip fault zones with a wide range of displacements: A field study from the Atacama fault system, northern Chile, J. Struct. Geol., 31(8), 802–816, doi:10.1016/j.jsg.2009.05.002, 2009.

Mitchell, T. M. and Toy, V. G.: Photograph of the month, J. Struct. Geol., 61, 143, doi:10.1016/j.jsg.2014.01.004, 2014.

Muir-Wood, R. and King, G. C. P.: Hydrological signatures of earthquake strain, J. Geophys. Res., 98(B12), 22035, doi:10.1029/93JB02219, 1993.

Nasseri, M. H. B., Rao, K. S. and Ramamurthy, T.: Anisotropic strength and deformation behavior of Himalayan schists, Int. J. Rock Mech. Min. Sci., 40(1), 3–23, doi:10.1016/S1365-1609(02)00103-X, 2003.

Norris, R. J. and Cooper, A. F.: Origin of small-scale segmentation and transpressional thrusting along the Alpine Fault, New Zealand, Geol. Soc. Am. Bull., 107(2), 231–240, doi:10.1130/0016-7606(1995)107<0231:OOSSSA>2.3.CO;2, 1995.

Norris, R. J. and Cooper, A. F.: Erosional control on the structural evolution of a transpressional thrust complex on the Alpine fault, New Zealand, J. Struct. Geol., 19(10), 1323–1342, doi:10.1016/S0191-8141(97)00036-9, 1997.

Norris, R. J. and Cooper, A. F.: Late Quaternary slip rates and slip-partitioning on the Alpine Fault, New Zealand, J. Struct. Geol., 23(2000), 507–520, 2001.

Norris, R. J. and Cooper, A. F.: Very high strains recorded in mylonites along the Alpine Fault, New Zealand: implications for the deep structure of plate boundary faults, J. Struct. Geol., 25(12), 2141–2157, 2003.

Norris, R. J. and Cooper, A. F.: The Alpine Fault, New Zealand: Surface Geology and Field Relationships, in A Continental Plate Boundary: Tectonics at South Island, New Zealand, edited by D. Okaya, T. A. Stern, and F. Davey, pp. 157–175, American Geophysical Union., 2007.

Norris, R. J. and Toy, V. G.: Continental transforms: A view from the Alpine Fault, J. Struct. Geol., 64, 3–31, doi:10.1016/j.jsg.2014.03.003, 2014.

O'Brien, G. A., Cox, S. C. and Townend, J.: Spatially and temporally systematic hydrologic changes within large geoengineered landslides, Cromwell Gorge, New Zealand, induced by multiple regional earthquakes, J. Geophys. Res. Solid Earth, 121(12), 8750–8773, 2016.

Paterson, M. S. and Wong, T. F.: Experimental rock deformation - The brittle field, Springer-Verlag Berlin Heidelberg., 2005.

Paulsen, T. S., Jarrard, R. D. and Wilson, T. J.: A simple method for orienting drill core by correlating features in whole-core scans and oriented borehole-wall imagery, J. Struct. Geol., 24(8), 1233–1238, doi:10.1016/S0191-8141(01)00133-X, 2002.

Peacock, D. C. P. and Sanderson, D. J.: Effects of layering and anisotropy on fault geometry, J. Geol. Soc. London., 149(5), 793–802, doi:10.1144/gsjgs.149.5.0793, 1992.

Price, N. J.: Mechanics of jointing in rocks, Geol. Mag., 96(2), 149–167, doi:10.1017/S0016756800060040, 1959.

Priest, S.: Discontinuity Analysis for Rock Engineering, Springer Science & Business Media., 1993.

Rattenbury, M. and Isaac, M.: The QMAP 1:250 000 Geological Map of New Zealand project, New Zeal. J. Geol. Geophys., 8306(April), doi:10.1080/00288306.2012.725417, 2012.

Reed, J. J.: Mylonites, cataclasites, and associated rocks along the Alpine fault, South Island, New Zealand, New Zeal. J. Geol. Geophys., 7(4), 645–684, doi:10.1080/00288306.1964.10428124, 1964.

Rice, J. R., Sammis, C. G. and Parsons, R.: Off-fault secondary failure induced by a dynamic slip pulse, Bull. Seismol. Soc. Am., 95(1), 109–134, doi:10.1785/0120030166, 2005.

Savage, E.: Investigating Rock Mass Conditions and Implications for Tunnelling and Construction of the Amethyst Hydro Project, Harihari, University of Canterbury., 2013.

Savage, H. M. and Brodsky, E. E.: Collateral damage: Evolution with displacement of fracture distribution and secondary fault strands in fault damage zones, J. Geophys. Res. Solid Earth, 116(3), doi:10.1029/2010JB007665, 2011.

Savage, H. M., Keranen, K. M., Schaff, D. and Dieck, C.: Possible Precursory Signals in

Damage Zone Foreshocks, Geophys. Res. Lett., 2017.

Schulz, S. E. and Evans, J. P.: Mesoscopic structure of the Punchbowl Fault, Southern California and the geologic and geophysical structure of active strike-slip faults, J. Struct. Geol., 22(7), 913–930, doi:10.1016/S0191-8141(00)00019-5, 2000.

Shigematsu, N., Otsubo, M., Fujimoto, K. and Tanaka, N.: Orienting drill core using borehole-wall image correlation analysis, J. Struct. Geol., 67(PB), 293–299, doi:10.1016/j.jsg.2014.01.016, 2014.

Sibson, R. H.: Earthquake faulting as a structural process, J. Struct. Geol., 11(1–2), 1–14, doi:10.1016/0191-8141(89)90032-1, 1989.

Sibson, R. H., White, S. H. and Atkinson, B. K.: Structure and distribution of fault rocks in the Alpine Fault Zone, New Zealand, Geol. Soc. London, Spec. Publ., 9(1), 197–210, 1981.

Simpson, G. D. H., Cooper, A. F. and Norris, R. J.: Late Quaternary evolution of the Alpine Fault Zone at Paringa, South Westland, New Zealand, New Zeal. J. Geol. Geophys., 37(1), 49–58, doi:10.1080/00288306.1994.9514600, 1994.

Stanley, C. R. and Hooper, J. J.: POND: An Excel spreadsheet to obtain structural attitudes of planes from oriented drillcore, Comput. Geosci., 29(4), 531–537, doi:10.1016/S0098-3004(03)00033-5, 2003.

Stern, T., Okaya, D., Kleffmann, S., Scherwath, M., Henrys, S. and Davey, F.: Geophysical exploration and dynamics of the Alpine Fault Zone, A Cont. Plate Bound. Tectonics South Island, New Zeal. Geophys. Monogr. Ser. 175, 207–233, doi:10.1029/175GM11, 2007.

Sutherland, R., Eberhart-Phillips, D., Harris, R. A., Stern, T., Beavan, J., Ellis, S., Henrys, S., Cox, S., Norris, R. J., Berryman, K. R., Townend, J., Bannister, S., Pettinga, J., Leitner, B., Wallace, L., Little, T. A., Cooper, A. F., Yetton, M. and Stirling, M.: Do Great Earthquakes Occur on the Alpine Fault in Central South Island, New Zealand?, in A Continental Plate Boundary: Tectonics at South Island, New Zealand, vol. 175, edited by D. Okaya, Stern, T., and F. Davey, pp. 235–251, American Geophysical Union., 2007.

Sutherland, R., Toy, V. G., Townend, J., Cox, S. C., Eccles, J. D., Faulkner, D. R., Prior, D. J., Norris, R. J., Mariani, E., Boulton, C., Carpenter, B. M., Menzies, C. D., Little, T. A., Hasting, M., De Pascale, G. P., Langridge, R. M., Scott, H. R., Reid Lindroos, Z., Fleming, B. and Kopf, J.: Drilling reveals fluid control on architecture and rupture of the Alpine fault, New Zealand, Geology, 40(12), 1143–1146, doi:10.1130/G33614.1, 2012.

Sutherland, R., Townend, J., Toy, V. G., Upton, P., Coussens, J. and DFDP2, S. T.: Extreme hydrothermal conditions at an active plate-bounding fault, Nature, 546, 137–140, doi:10.1038/nature22355, 2017.

Sylvester, A. G.: Strike-Slip Faults, Geol. Soc. Am. Bull., 100(November), 1666–1703, doi:10.1130/0016-7606(1988)100<1666:SSF>2.3.CO;2, 1988.

Templeton, E. L., Rice, J. R., Viesca, R. C., Templeton, E. L. and Rice, J. R.: Off-fault plasticity and earthquake rupture dynamics: 2. Effects of fluid saturation, J. Geophys. Res. Solid Earth, 113(9), doi:10.1029/2007JB005530, 2008.

Terzaghi, R. D.: Sources of Error in Joint Surveys, Géotechnique, 15(3), 287–304, doi:10.1680/geot.1965.15.3.287, 1965.

Tippett, J. M. and Kamp, P. J. J.: Quantitative relationships between uplift and relief parameters for the Southern Alps, New Zealand, as determined by fission track analysis, Earth Surf. Process. Landforms, 20(2), 153–175, 1995.

Townend, J. and Zoback, M. D.: How faulting keeps the crust strong, Geology, 28(5), 399–402, doi:10.1130/0091-7613(2000)28<399:HFKTCS>2.0.CO, 2000.

Townend, J., Sutherland, R., Toy, V. G., Eccles, J. D., Boulton, C., Cox, S. C. and McNamara, D.: Late-interseismic state of a continental plate-bounding fault: Petrophysical results from DFDP-1 wireline logging and core analysis, Alpine Fault, New Zealand, Geochemistry, Geophys. Geosystems, 14(9), 3801–3820, doi:10.1002/ggge.20236, 2013.

Townend, J., Sutherland, R., Toy, V. G., Doan, M. L., Célérier, B., Massiot, C., Coussens, J., Jeppson, T., Janku-Capova, L., Remaud, L., Upton, P., Schmitt, D. R., Pezard, P., Williams, J., Allen, M. J., Baratin, L. M., Barth, N., Becroft, L., Boese, C. M., Boulton, C., Broderick, N., Carpenter, B., Chamberlain, C. J., Cooper, A., Coutts, A., Cox, S. C., Craw, L., Eccles, J. D., Faulkner, D., Grieve, J., Grochowski, J., Gulley, A., Hartog, A., Henry, G., Howarth, J., Jacobs, K., Kato, N., Keys, S., Kirilova, M., Kometani, Y., Langridge, R., Lin, W., Little, T., Lukacs, A., Mallyon, D., Mariani, E., Mathewson, L., Melosh, B., Menzies, C., Moore, J., Morales, L., Mori, H., Niemeijer, A., Nishikawa, O., Nitsch, O., Paris, J., Prior, D. J., Sauer, K., Savage, M. K., Schleicher, A., Shigematsu, N., Taylor-Offord, S., Teagle, D., Tobin, H., Valdez, R., Weaver, K., Wiersberg, T. and Zimmer, M.: Petrophysical, Geochemical, and Hydrological Evidence for Extensive Fracture-Mediated Fluid and Heat Transport in the Alpine Fault's Hanging-Wall Damage Zone, Geochemistry, Geophys. Geosystems, 18(12), 4709–4732, doi:10.1002/2017GC007202, 2017.

Toy, V.: Rheology of the Alpine Fault mylonite zone: deformation processes at and below the base of the seismogenic zone in a major plate boundary structure, University of Otago., 2008.

Toy, V. G., Prior, D. J. and Norris, R. J.: Quartz fabrics in the Alpine Fault mylonites: Influence of pre-existing preferred orientations on fabric development during progressive uplift, J. Struct. Geol., 30(5), 602–621, doi:10.1016/j.jsg.2008.01.001, 2008.

Toy, V. G., Craw, D., Cooper, A. F. and Norris, R. J.: Thermal regime in the central Alpine Fault zone, New Zealand: Constraints from microstructures, biotite chemistry and fluid inclusion data, Tectonophysics, 485(1–4), 178–192, doi:10.1016/j.tecto.2009.12.013, 2010.

Toy, V. G., Boulton, C. J., Sutherland, R., Townend, J., Norris, R. J., Little, T. A., Prior, D. J., Mariani, E., Faulkner, D., Menzies, C. D., Scott, H. and Carpenter, B. M.: Fault rock lithologies and architecture of the central Alpine fault, New Zealand, revealed by DFDP-1 drilling, Lithosphere, 7(2), 155–173, doi:10.1130/l395.1, 2015.

Toy, V. G., Sutherland, R., Townend, J., Allen, M. J., Becroft, L., Boles, A., Boulton, C., Carpenter, B., Cooper, A., Cox, S. C., Daube, C., Faulkner, D. R., Halfpenny, A., Kato, N., Keys, S., Kirilova, M., Kometani, Y., Little, T., Mariani, E., Melosh, B., Menzies, C. D., Morales, L., Morgan, C., Mori, H., Niemeijer, A., Norris, R., Prior, D., Sauer, K., Schleicher, A. M., Shigematsu, N., Teagle, D. A. H., Tobin, H., Valdez, R., Williams, J., Yeo, S., Baratin, L. M., Barth, N., Benson, A., Boese, C., Célérier, B., Chamberlain, C. J., Conze, R., Coussens, J., Craw, L., Doan, M. L., Eccles, J., Grieve, J., Grochowski, J., Gulley, A., Howarth, J., Jacobs, K., Janku-Capova, L., Jeppson, T., Langridge, R., Mallyon, D., Marx, R., Massiot, C., Mathewson, L., Moore, J., Nishikawa, O., Pooley, B., Pyne, A., Savage, M. K., Schmitt, D., Taylor-Offord, S., Upton, P., Weaver, K. C., Wiersberg, T. and Zimmer, M.: Bedrock geology of DFDP-2B, central Alpine Fault, New Zealand, New Zeal. J. Geol. Geophys., 60(4), 497–518, doi:10.1080/00288306.2017.1375533, 2017.

Turnbull, I. M., Mortimer, N. and Craw, D.: Textural zones in the Haast Schist—a reappraisal, New Zeal. J. Geol. Geophys., 44(1), 171–183, doi:10.1080/00288306.2001.9514933, 2001.

Upton, P., Song, B. R. and Koons, P. O.: Topographic control on shallow fault structure and strain partitioning near Whataroa, New Zealand demonstrates weak Alpine Fault, New Zeal. J. Geol. Geophys., 1–8, doi:10.1080/00288306.2017.1397706, 2017.

Vermilye, J. M. and Scholz, C. H.: The process zone: A microstructural view of fault growth, J. Geophys. Res. Earth, 103(B6), 12223–12237, doi:10.1029/98JB00957, 1998.

Warr, L. N. and Cox, S.: Clay mineral transformations and weakening mechanisms along the Alpine Fault, New Zealand, in Geological Society, London, Special Publications, vol. 186, edited by R. E. Holdsworth, R. A. Strachan, J. F. Magloughlin, and R. J. Knipe, pp. 85–101, The Geological Society, London., 2001.

Wellman, H.: Data for the Study of Recent and Late Pleistocene Faulting in the South, New Zeal. J. Sci. Technol., 34(4), 270–288, 1953.

Williams, J. N., Toy, V. G., Massiot, C., McNamara, D. D. and Wang, T.: Damaged beyond repair? Characterising the damage zone of a fault late in its interseismic cycle, the Alpine Fault, New Zealand, J. Struct. Geol., 90, 76–94, doi:10.1016/j.jsg.2016.07.006, 2016.

Williams, J. N., Toy, V. G., Smith, S. A. F. and Boulton, C.: Fracturing, fluid-rock interaction and mineralisation during the seismic cycle along the Alpine Fault, J. Struct. Geol., 103, 151–166, doi:https://doi.org/10.1016/j.jsg.2017.09.011, 2017a.

Williams, J. N., Toy, V. G., Massiot, C. and McNamara, D.: X-ray Computed Tomography and borehole televiewer images of the Alpine Fault's hanging-wall, New Zealand: Deep Fault Drilling Project phase 1 (DFDP-1) and Amethyst Hydro Project (AHP), GFZ Data Serv., doi:http://doi.org/10.5880/ICDP.5052.004, 2017b.

Wilson, J. E., Chester, J. S. and Chester, F. M.: Microfracture analysis of fault growth and wear processes, Punchbowl Fault, San Andreas system, California, J. Struct. Geol., 25(11), 1855–1873, doi:10.1016/S0191-8141(03)00036-1, 2003.

Wright, C. A.: Geology and paleoseismicity of the central Alpine Fault, New Zealand., 1998.

Yukutake, Y., Ito, H., Honda, R., Harada, M., Tanada, T. and Yoshida, A.: Fluid-induced swarm earthquake sequence revealed by precisely determined hypocenters and focal mechanisms in the 2009 activity at Hakone volcano, Japan, J. Geophys. Res. Solid Earth, 116(4), doi:10.1029/2010JB008036, 2011.

Zangerl, C., Loew, S. and Eberhardt, E.: Structure, geometry and formation of brittle discontinuities in anisotropic crystalline rocks of the central Gotthard massif, Switzerland, Eclogae Geol. Helv., 99(2), 271–290, doi:10.1007/s00015-006-1190-0, 2006.

List of Figures

Figure 1

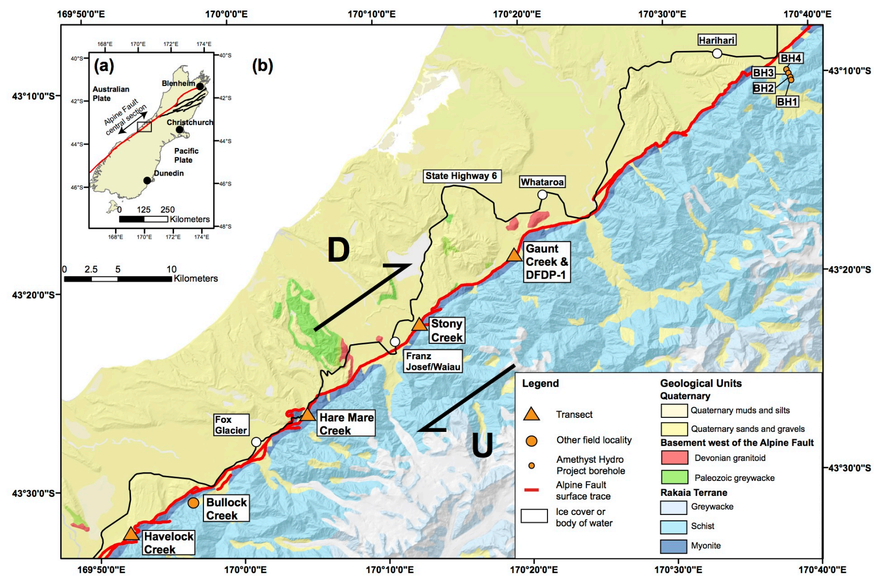

Figure 1: (a) Location map for Alpine Fault (red line) and Marlborough Faults (black line) in the South Island of New Zealand. Box shows extent of (b), a location map for the DFDP-1 and AHP boreholes, and field transects. The generalised underlying geology is derived from the GNS Science 1:250000 QMAP project (Rattenbury and Isaac, 2012) and has been draped over a digital elevation model (Columbus et al., 2011).

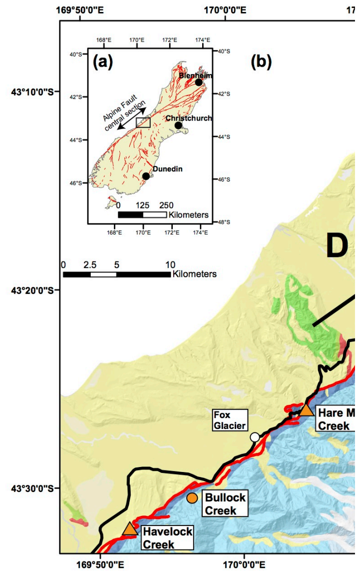

Deleted:

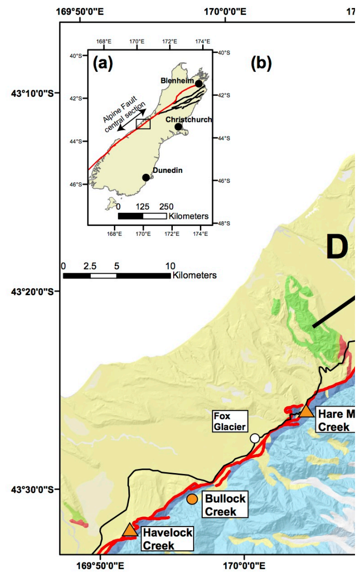

Deleted:

Deleted: and all other onshore active faults

Deleted: onin

Deleted: (GNS Science Active Fault Database, http://data.gns.cri.nz/af/).

Figure 2

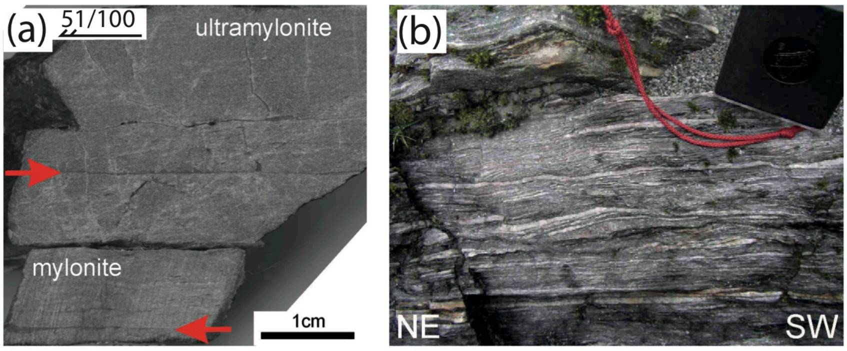

Figure 2: (a) Quartzofeldspathic Alpine Fault ultramylonite that gradually grades to mylonite at the base of the image. A foliation defined by alternating white quartzofeldspathic bands and dark grey mica bands is hard to distinguish in the ultramylonite but is more apparent in the mylonite. (b) The well foliated Alpine Fault protomylonite-mylonite transition. Compass is 5 cm wide. Both images previously presented in Toy, (2008). The sample in (a) was taken from Gaunt Creek, as was the photo in (b).

Deleted: ultramylonite, but

Deleted: W

Deleted: at Gaunt Creek

Deleted: The s

Deleted: was

Deleted: as was the

Figure 3

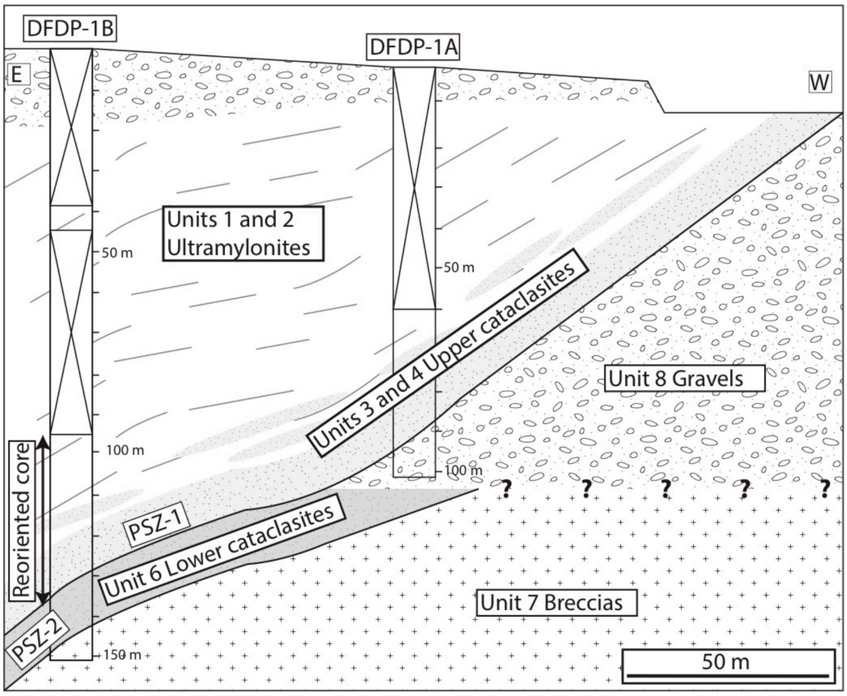

Figure 3: Cross section through the DFDP-1 boreholes, showing interval where reoriented drill-core is located. Boxes with diagonal lines depict intervals in borehole with no core recovery, grey lines represent mylonitic foliation. Modified from Sutherland et al., (2012), with lithological units previously defined by Toy et al., (2015).

Figure 4

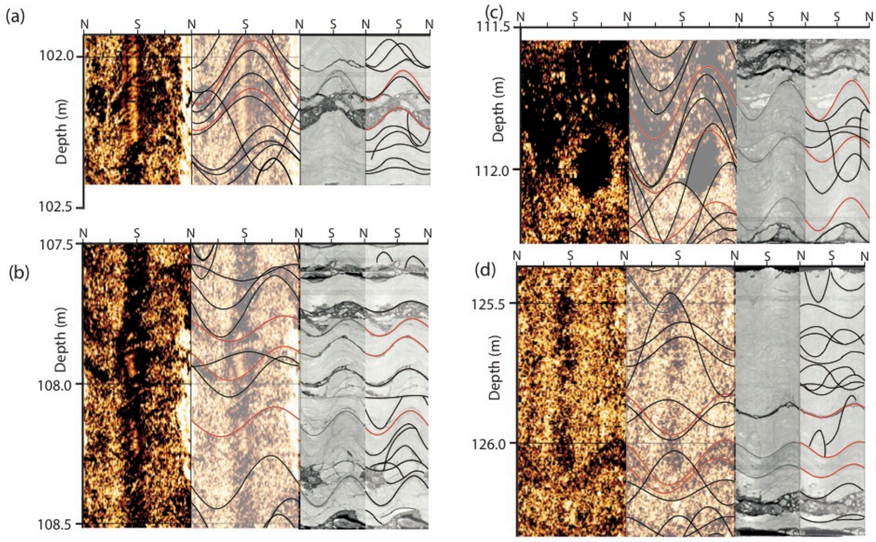

Figure 4: Examples of matching structures between BHTV images and unrolled CT images. In each image, the first two columns are the BHTV amplitude image, without and with interpretations respectively, whilst the third and fourth columns depict the unrolled CT image over the same interval, also without and with interpretations. Fractures that have been traced in red indicate those that were matched to reorientate core.

Figure 5

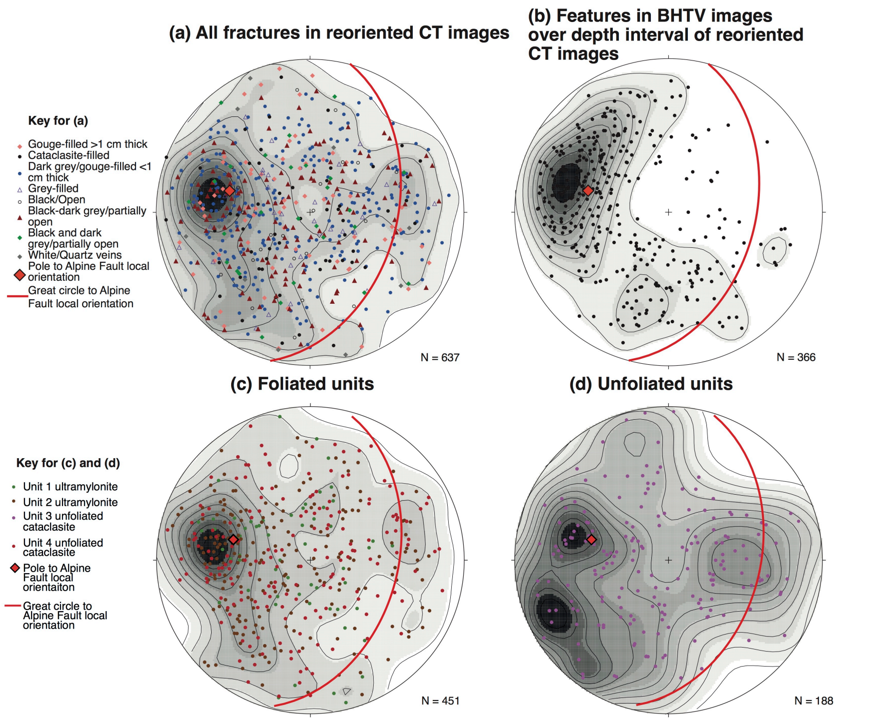

Figure 5: Lower hemisphere equal area stereplots depicting orientation of fractures in DFDP-1. Contouring on stereoplots was applied to poles that are weighted depending on their orientation correction *w* (see Sect. 3.2), and that are rounded to the nearest whole number. Contours were then generated for the weighted poles using a probability distribution calculated by a Kernel function in the RFOC package for R (Lees, 2014). Great circle represents orientation of Alpine Fault plane and foliation at DFDP-1 site (Townend et al., 2013). (a) Orientation of all fractures that were reoriented by matching structures between unrolled CT images and BHTV images, sorted by fracture type (Williams et al., 2016). (b) Orientation of features recognised in the BHTV images over the interval of reoriented core (94-126 m in DFDP-1B). Fracture orientations extracted from reoriented DFDP-1 CT images in (c) foliated units and (d) unfoliated units, using the DFDP-1 lithological classification scheme (Toy et al., 2015).

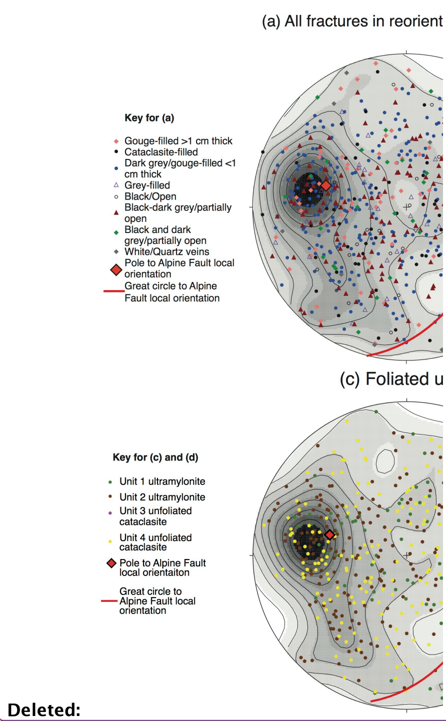

Deleted:

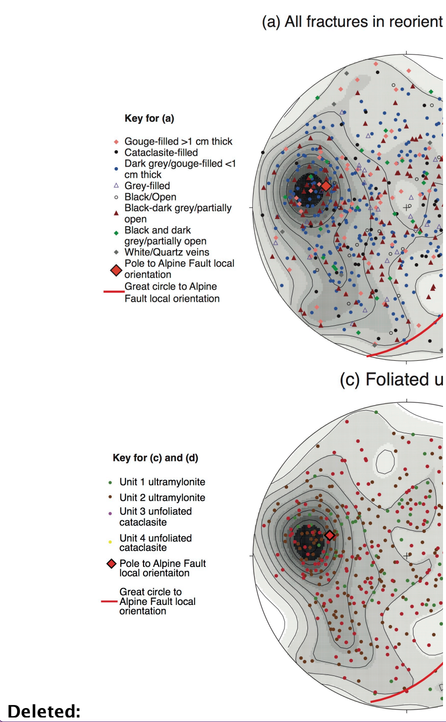

Deleted:

Figure 6

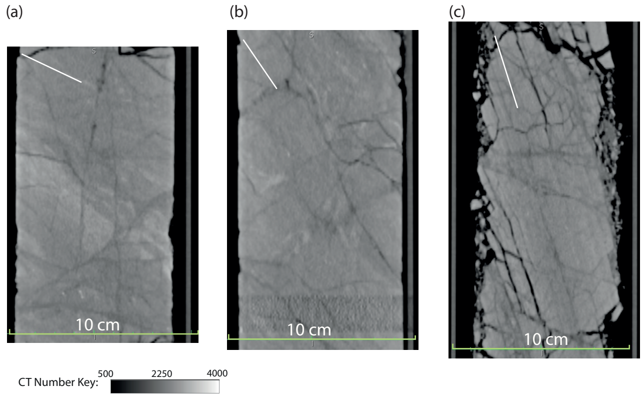

Figure 6: The relationship between foliation and fracture orientations in Alpine Fault ultramylonite, as observed in 2D CT image slices of DFDP-1 drill-core. Intervals are (borehole, core section and run, depth interval): (a) DFDP-1A 55-1 75.45-75.62 m, (b) DFDP-1B 35-1 102.49-102.64 m, and (c) DFDP-1B 25-2, 44.80-45.20 m. In (a) and (b) fractures tend to cross-cut the ultramylonitic foliation (orientation represented by white line in top left corner of each image). (c) Fractures show a greater preference to be aligned parallel to the foliation. Note that (c) was previously shown in Williams et al., (2016), and is not included in the reorientation analysis in Figure 5, as there was no BHTV imagery for this interval.

Moved (insertion) [1]

Moved up [1]: Intervals are (borehole, core section and run, depth interval): (a) DFDP-1A 55-1 75.45-75.62 m, (b) DFDP-1B 35-1 102.49-102.64 m, and (c) DFDP-1B 25-2, 44.80-45.20 m.

Figure 7

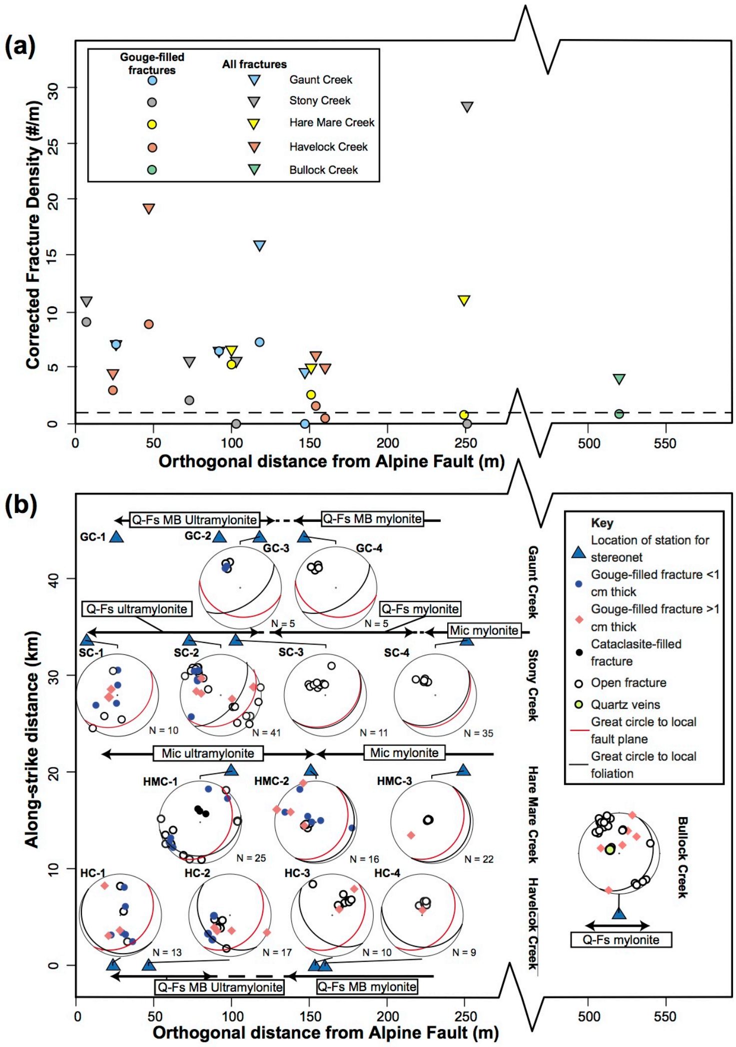

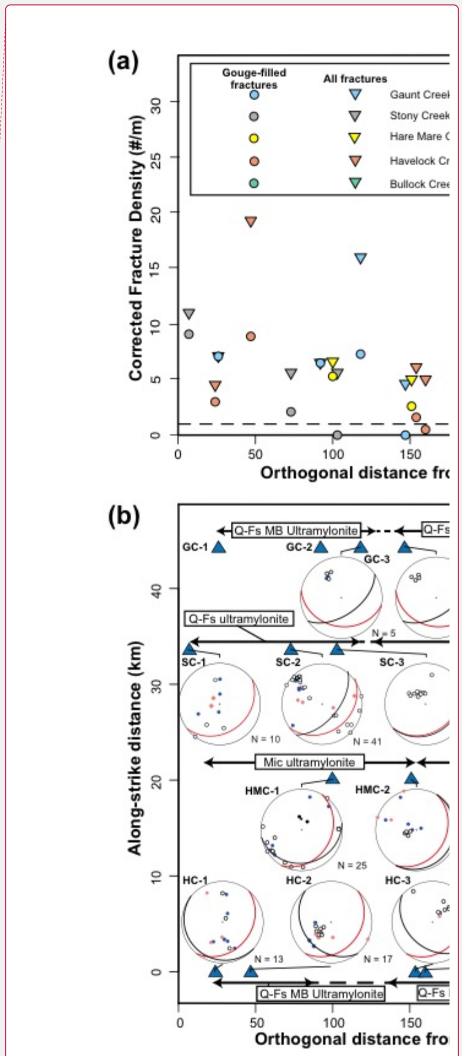

Deleted:

Figure 7: (a) Corrected fracture density at all stations for gouge-filled fractures and all fractures. Dashed line indicates a corrected fracture density of 1 fracture/metre. No orientation data was collected at Gaunt Creek stations 1 and 2, so fracture density is calculated from the two perpendicular transects. (b) Compilation of stereoplots for fracture orientations at each field station. Stations have

been plotted as a function of distance from the fault and distance along-strike (with respect to Havelock Creek) along within fault rock lithologies. Dashed lines indicate gradational or obscured lithological boundaries. Qfs, Quartzofeldspath; MB, metabasic; Mic, Micaceous. For field cross sections and location of stations, see Figure S1. Results are also summarised in Table S2.

Figure 8

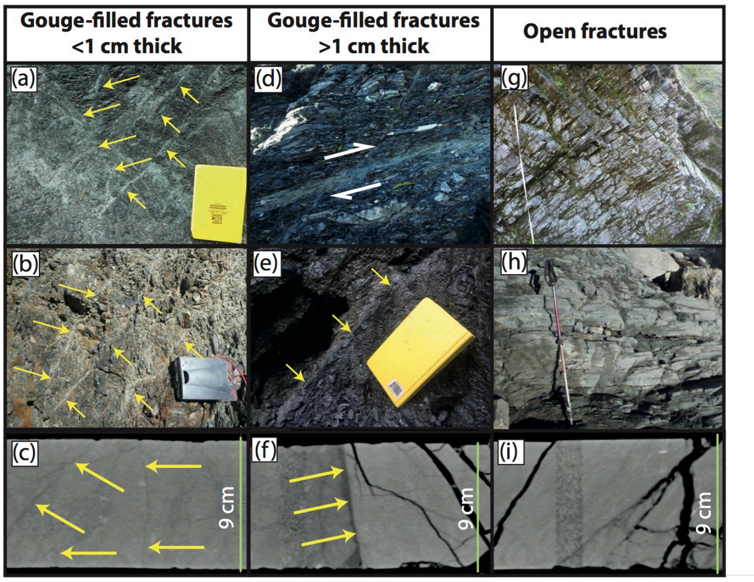

Figure 8: Examples of the three main types of fractures observed in the field around the Alpine Fault, and correlative fractures in DFDP-1 CT scans. (a-c) Thin gouge-filled fractures (yellow arrows) have a range of orientations and found exclusively within 160 m from the fault. They are equivalent to type iii of fractures from Williams et al., (2016). (d-f) Thicker gouge and cataclasite filled fractures are equivalent to type i and ii fractures of Williams et al. (2016) and may be observed at all distances from the Alpine Fault. Offset markers can be observed across these fractures (e.g. the vein indicated by the pen and white arrows in (d)). (g-i) Open fractures are mainly foliation-parallel. Equivalent to type v fractures of Williams et al., (2016). Location of field photos: (a) Waikukupa thrust, (b) and (g) Stony Creek, (d) and (h) Havelock Creek, (e) Bullock Creek. Compass clinometer 8 cm and yellow notebook 20 cm in length. Measuring tape in (e) 1.1 m long, walking pole in (g) 1 m in length. DFDP-1 CT scan intervals: (c) DFDP-1B 56-2 125.35-125.49 m, (f) DFDP-1B 35-1 102.00-102.15 m, (i) DFDP-1B 33-2 99.45-99.60 m

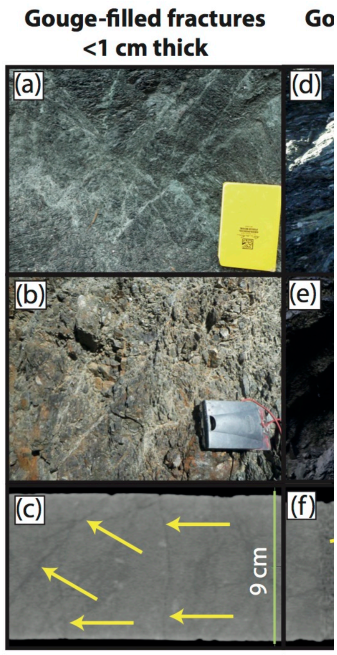

Deleted:

Deleted: different

Figure 9

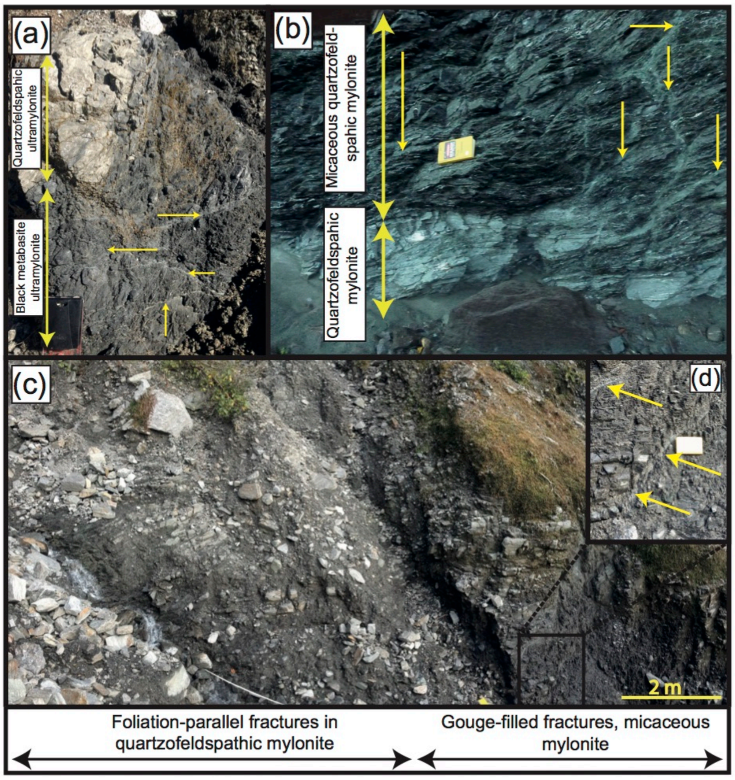

Figure 9: Field observations of changes in fracture density at lithological contacts. (a&b) Intervals of micaceous and metabasite mylonite containing a relatively high proportion of gouge filled fractures (denoted by yellow arrows) compared to interlayered quartzofeldspathic mylonite. (c) Transition from micaceous mylonite to quartzofeldspathic mylonite coincides with furthest extent of intensive gouge-filled fractures, as shown by yellow arrows in (d). Taken at (a) Gaunt Creek, (b) Havelock Creek, (c&d) Hare Mare Creek. Compass clinometer 8 cm and yellow notebook 20 cm in length.

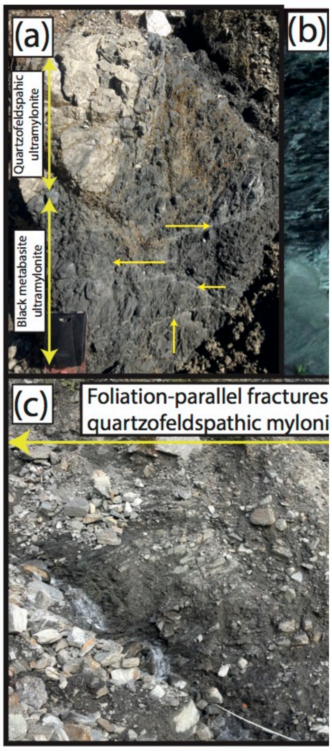

Deleted:

Deleted:

Formatted: Font:Times New Roman, 11 pt, Not Italic, Font color: Auto

Deleted: variations in fracture density coincident with lithological diversity

Deleted:

Deleted: ing

Figure 10

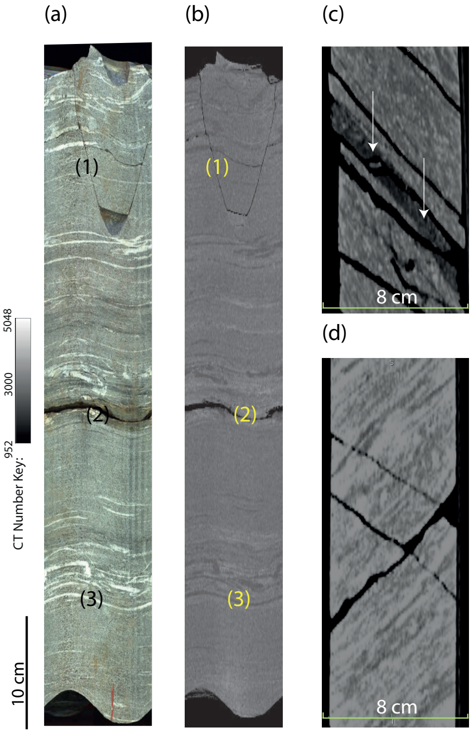

Figure 10: Fractures noted in the Amethyst Hydro Project (AHP) drill-core. Unrolled images of AHP drill-core (BH1 45-2 124.3-124.9 m) taken by (a) DMT core scanner and (b) generated from a CT image. (1) Identifies fracture cutting across foliation, (2) foliation-parallel fracture with alteration halo, (3) foliation defined by quartzofeldspathic bands that have low CT numbers. (c&d) Core-axial parallel CT image slices of AHP drill-core. In (c) white arrows point to a 'crush zone' sub parallel to foliation (BH2 75-2 155.92-156.04 m). (d) more variable fracture orientations identified in BH4 (Section 70-4 196.62-196.80 m).

Deleted: styles

Figure 11

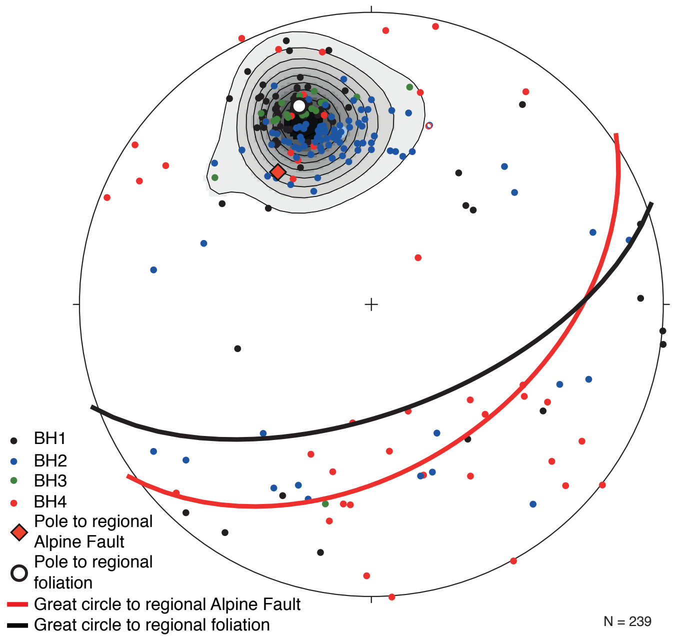

Figure 11: Equal area, lower hemisphere projection of fracture orientations recognised in CT scans of AHP drill-core separated by borehole. Contours plotted with weighted poles (see Figure 5).

Figure 12

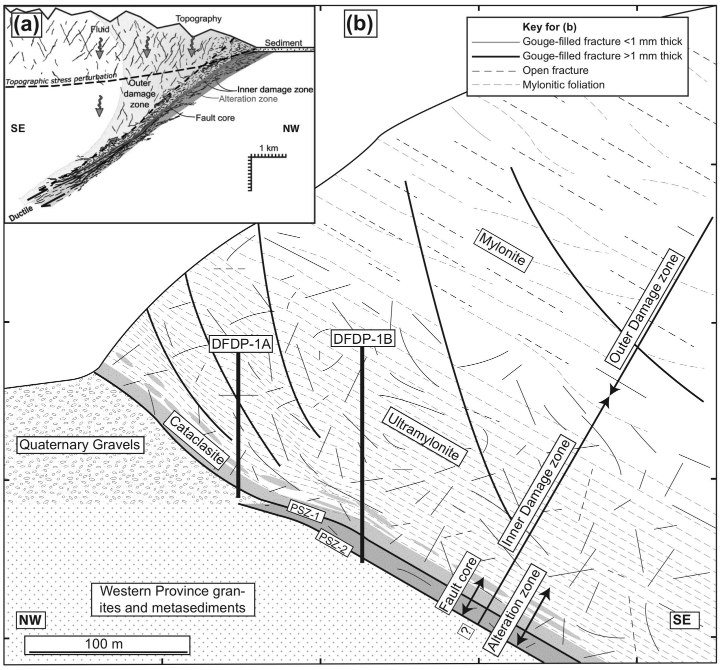

Figure 12: Schematic cross sections through the Alpine Fault illustrating its hanging-wall structure. (a) Crustal-scale cross section illustrating the flower shaped geometry of the outer damage zone (after Townend et al., (2017)). (b) A thrust section within the central section of the Alpine Fault, depicting fracture network, its relationship to foliation, and the distribution of subsidiary faults. Respective position of DFDP-1 boreholes also shown. Constructed from cross sections previously presented in Norris and Cooper, (2007) and Sutherland et al., (2012).

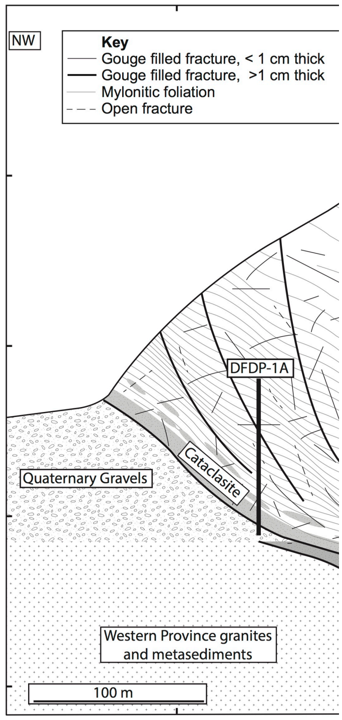

Deleted:

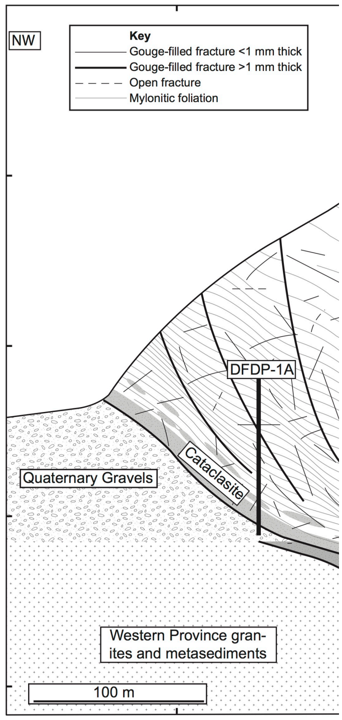

Deleted:

Deleted: A s…hematic cross sectionsn…through th … [7]

Figure 13

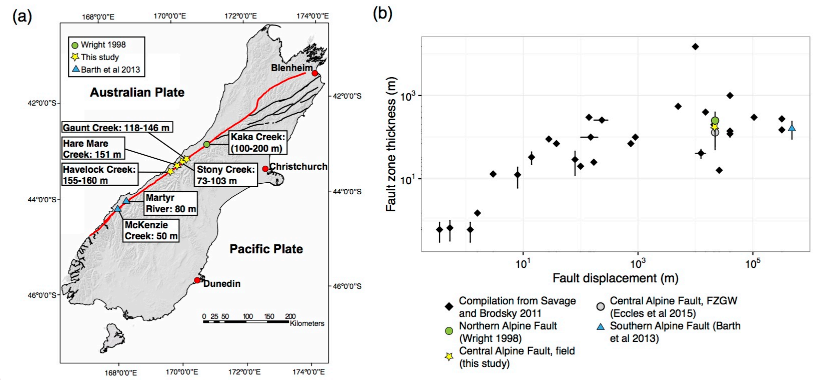

Figure 13: (a) Compilation of estimates of the 'inner damage zone' width on the Pacific Plate side of the Alpine Fault (red line) from four creek sections in this study (Gaunt Creek, Stony Creek, Hare Mare Creek and Havelock Creek). This is combined with other along-strike estimates of damage zone thickness for the Pacific Plate side of the Alpine Fault: McKenzie Creek and Martyr River (Barth et al., 2013) and Kaka Creek (Wright, 1998). (b) Log-log plot of fault zone thickness as a function of fault displacement previously presented in Savage and Brodsky, (2011), combined with estimates made for the Alpine Fault assuming footwall damage is no more extensive than in the hanging-wall. Displacement for the Alpine Fault is 480 km (Norris and Cooper, 2007; Wellman, 1953). However, convergence along the Alpine Fault's central section requires that it erodes its own fault rocks so these points are plotted to reflect only the brittle displacement the rocks themselves have accommodated as they are exhumed through the seismogenic zone (22 km, Barth et al., (2012)). Error bars reflect uncertainty in constraining fault zone width (as for example, footwall damage is largely unknown), not necessarily variability in fault zone thickness.

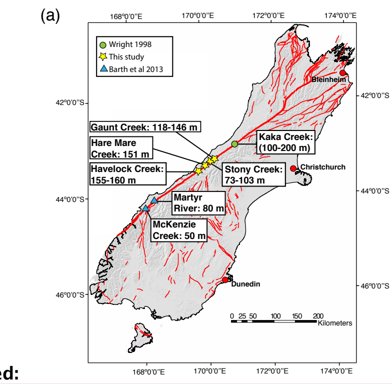

Deleted:

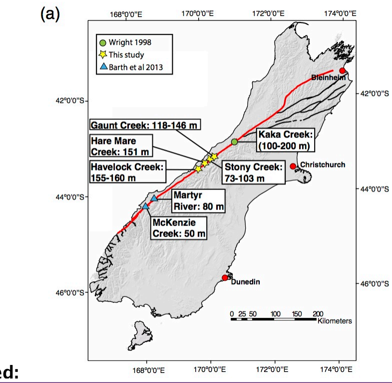

Deleted:

Deleted:

Deleted: extent of intensive gouge-filled fracturing

Deleted: , which is considered to be the best indicator of Alpine Fault damage zone width.

Deleted: ,

Figure A1

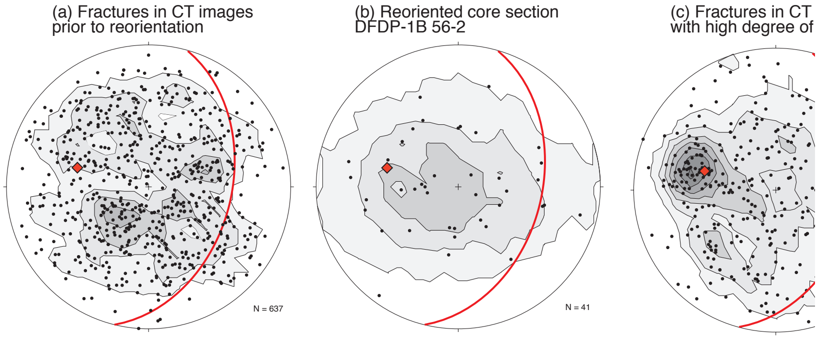

Figure A1: Stereoplots to tests the confidence in reorientations applied to rotate DFDP-1 CT scan fracture orientations into geographic coordinates. Red great circle and diamond in each plot represents plane and pole to the Alpine Fault orientation measured in DFDP-1B. Plotted with Kamb contours with intervals of two standard deviations. (a) Orientation of fractures shown in Figure 5a before rotation, (b) orientation of reoriented fractures within a single core section (DFDP-1B 56-2), and (c) orientation of fractures in CT images from core sections that were oriented with a high degree of confidence with BHTV images.

List of Tables

Table 1

	Number of fractures	Resultant Plane dip direction	Resultant Plane dip	Resultant vector length (Cluster intensity, 2 s.f.)
All reoriented DFDP-1 CT fractures	637	80	58	0.58
Reoriented DFDP-1 CT fractures, foliated units	451	87	58	0.58
Reoriented DFDP-1 CT fractures, unfoliated units	188	71	61	0.58
DFDP-1B BHTV features (depth interval 94-126 m)	365	103	47	0.72
AHP Fractures	239	164	58	0.76

Table 1: Clustering analysis of the different fracture datasets documented in this study, using the resultant vector methodology outlined by Priest, (1993). DFDP-1 foliated units comprise ultramylonites and foliated cataclasites (Units 1, 2 and 4 of Toy et al., (2015)). DFDP-1

Formatted: Font:Bold

Formatted: Normal

Deleted: (

unfoliated units comprise unfoliated cataclasites (Unit 3 of Toy et al., (2015)). The resultant vector orientation for each dataset, which has been converted to spherical coordinates, is also reported. See text for full details.

Deleted: which

Formatted: Font:Not Bold

Page 19: [1] Deleted	Microsoft Office User	30/12/2017 12:04:00

Projections of outcrop-derived measurements (Norris and Cooper, 1995, 2007)

Page 23: [2] Deleted	Microsoft Office User	25/02/2018 12:07:00

Page 27: [3] Deleted	Microsoft Office User	31/12/2017 12:52:00

Page 28: [4] Deleted	Microsoft Office User	28/02/2018 21:29:00

Page 30: [5] Deleted	Microsoft Office User	31/12/2017 11:39:00

Gouge-filled fractures are present at all distances in our field transects (Figure 7-9) and within the AHP drill-core (Figure 10c). However, their interval of high density (>1 fracture/metre) is restricted to less than 118-147 m from the PSZs at Gaunt Creek (i.e. between stations 3-4), <73-103 m at Stony Creek (i.e. between stations 2-3), <151 m at Hare Mare Creek (at station 2, Figure 8c) and <154-160 m at Havelock Creek (i.e. between stations 3-4). This is consistent with the observations of Norris and Cooper, (2007) who suggested that the Alpine Fault's central section damage zone can be defined by a ~100 m wide zone of intensive gouge-filled fractures. These estimates of damage zone width are also similar to those made elsewhere on the Alpine Fault (e.g. Barth et al., 2013 in the southern section in South Westland; Wright, 1998 at the northern end of the the central section, Figure 13a) and to other predictions for crustal-scale (Figure 13b), rapidly-moving (~few cm/yr) fault zones that have accommodated hundreds of kilometres of displacement (Biegel and Sammis, 2004; Childs et al., 2009; Finzi et al., 2009; Manighetti et al., 2007; Perrin et al., 2016; Savage and Brodsky, 2011; Savage and Cooke, 2010).

Page 31: [6] Deleted	Microsoft Office User	01/03/2018 15:26:00

FZGWs provide a measure of the total width of the damage zone. The width of the inner damage zone documented here from the hanging-wall of the Alpine Fault accounts for most of the LVZ detected by FZGWs. This implies that fracture damage around the Alpine Fault is dominantly hosted in the hanging wall, consistent with other dipping thrust faults (Li et al., 2013; Ma, 2009; Yeh et al., 2007). However, Western Province basement rocks to the west of the Alpine Fault are rarely exposed (Lund Snee et al., 2014; Norris and Cooper, 2007) and it remains unknown whether the Alpine Fault footwall is extensively fractured

Page 63: [7] Deleted	Microsoft Office User	01/03/2018 18:15:00

A s

Page 63: [7] Deleted	Microsoft Office User	01/03/2018 18:15:00

A s

Page 63: [7] Deleted	Microsoft Office User	01/03/2018 18:15:00

A s

Page 63: [7] Deleted	Microsoft Office User	01/03/2018 18:15:00

A s

Page 63: [7] Deleted	Microsoft Office User	01/03/2018 18:15:00

A s